Article

Cell Reports

The Exchangeable Apolipoprotein Nplp2 Sustains Lipid Flow and Heat Acclimation in *Drosophila*

Graphical Abstract

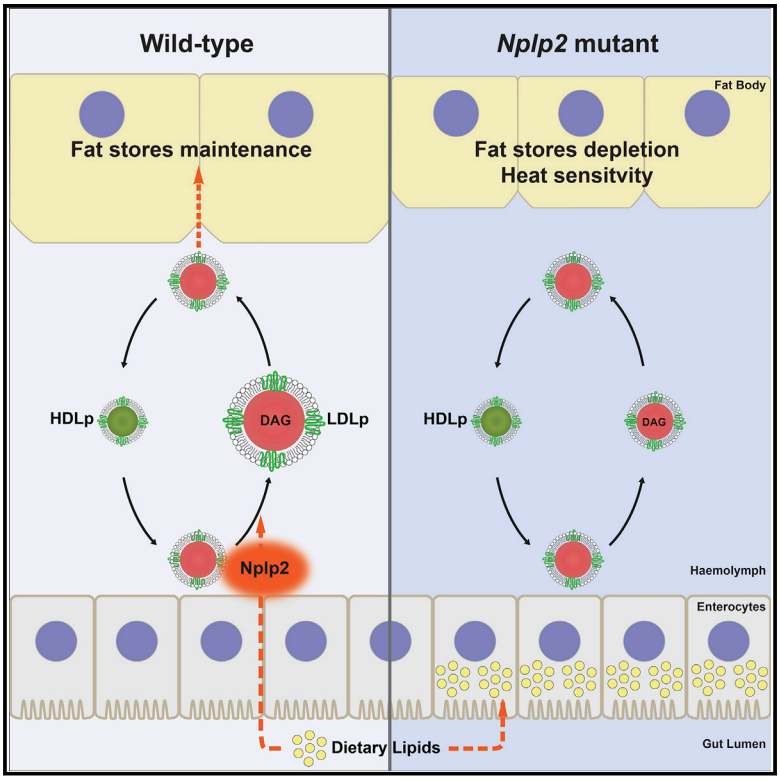

Authors

Samuel Rommelaere, Jean-Philippe Boquete, Jérémie Piton, Shu Kondo, Bruno Lemaitre

Correspondence

samuel.rommelaere@epfl.ch (S.R.), bruno.lemaitre@epfl.ch (B.L.)

In Brief

Rommelaere et al. identify a small exchangeable apolipoprotein in *Drosophila* that facilitates dietary lipid extraction and fat storage. Nplp2 sustains lipid flow to fuel the heat stress response, promoting insect survival at elevated temperatures. Optimization of lipid transport during stress via dedicated lipoproteins likely applies to other species including vertebrates.

Highlights

- We identified Nplp2, an exchangeable apolipoprotein in *Drosophila*
- Nplp2 maximizes Lipophorin lipid loading capacity
- Nplp2 controls dietary lipid extraction and optimal fat storage
- Nplp2 fuels the stress response with dietary lipids and promotes heat acclimation

Rommelaere et al., 2019, Cell Reports *27*, 886–899
April 16, 2019 © 2019 The Author(s).
https://doi.org/10.1016/j.celrep.2019.03.074

CellPress

OPEN ACCESS
CellPress

Cell Reports
Article

The Exchangeable Apolipoprotein Nplp2 Sustains Lipid Flow and Heat Acclimation in *Drosophila*

Samuel Rommelaere,[1,*] Jean-Philippe Boquete,[1] Jérémie Piton,[1] Shu Kondo,[2] and Bruno Lemaitre[1,3,*]
[1]Global Health Institute, School of Life Science, École Polytechnique Fédérale de Lausanne (EPFL), 1015 Lausanne, Switzerland
[2]Invertebrate Genetics Laboratory, Genetic Strains Research Center, National Institute of Genetics, Mishima 411-8540, Japan
[3]Lead Contact
*Correspondence: samuel.rommelaere@epfl.ch (S.R.), bruno.lemaitre@epfl.ch (B.L.)
https://doi.org/10.1016/j.celrep.2019.03.074

SUMMARY

In ectotherms, increased ambient temperature requires the organism to consume substantial amounts of energy to sustain a higher metabolic rate, prevent cellular damage, and respond to heat stress. Here, we identify a heat-inducible apolipoprotein required for thermal acclimation in *Drosophila*. Neuropeptide-like precursor 2 (Nplp2) is an abundant hemolymphatic protein thought to be a neuropeptide. In contrast, we show that Nplp2 contributes to lipid transport, functioning as an exchangeable apolipoprotein. More precisely, *Nplp2*-deficient flies accumulate lipids in their gut, have reduced fat stores, and display a dyslipoproteinemia, showing that Nplp2 is required for dietary lipid assimilation. Importantly, Nplp2 is induced upon thermal stress and contributes to survival upon heat stress. We propose that Nplp2 associates with lipoprotein particles under homeostatic and high energy-demand conditions to optimize fat transport and storage. Our study also shows that modulation of the lipid uptake and transport machinery is part of an integrated cytoprotective response.

INTRODUCTION

The last half century has been characterized by a global warming of the climate system, a phenomenon very likely to be a consequence of human industrial activity (IPCC, 2014). These changes are expected to have profound impacts on the biosphere. As ectotherms, insects have a limited capacity to regulate their body temperature and are therefore very sensitive to external temperature variations. As a result, numerous insect species are threatened by global warming (Martinet et al., 2015; Klok and Chown, 1997; Nyamukondiwa et al., 2013). Since insect pollinators are essential for maintaining natural biodiversity and agriculture, their extinction would have dramatic ecological and agricultural consequences (Fründ et al., 2013; Jevanandam et al., 2013). Insects may adapt to temperature increases using different strategies, including behavioral and metabolic adaptations. Understanding insect acclimation to warmer environments is therefore critical for predicting and managing the consequences of global warming.

Upon thermal stress exposure, several cytoprotective mechanisms are activated to limit tissue damage and promote the return to homeostasis. The most studied ones are heat shock proteins, which are highly induced after thermal challenge (Saibil, 2013). Because the stress response costs energy, it requires an appropriate energy supply. Moreover, the anabolic process accompanying tissue repair also needs to be sustained by nutrient influx. Studies in *Drosophila* have shown that heat stress depletes energy stores and has a prolonged effect on metabolite profile and fly fitness (Klepsatel et al., 2016; Sarup et al., 2016; Ryuda et al., 2018). So far, however, the molecular mechanisms underlying nutrient supply during heat stress and tissue repair remain poorly understood.

In insects, energy is stored as glycogen and triacylglycerides (TAGs). Upon energetic demand, glycogen is degraded and released as trehalose into the hemolymph, while TAGs are hydrolyzed into diacylglycerides (DAGs). DAGs are highly hydrophobic molecules that need to be packaged into lipoprotein particles for transport. Apolipoproteins serve as a scaffold for these particles but also mediate interactions with lipoprotein receptors and enzymes involved in their catabolism (Feingold and Grunfeld, 2000). Lipoprotein particles vary in size, lipid content, and apolipoprotein composition. Lipoprotein particles are classified according to their density, which reflects their lipid content, ranging from high-density-lipoprotein particles (HDLps) to low-density-lipoprotein particles (LDLps).

In *Drosophila,* the apoB-homolog lipophorin (Lpp) transports the bulk of lipids (Palm et al., 2012). Lpp is produced mostly by the fat body and released partially lipidated into the hemolymph. It transiently associates with enterocytes where lipid loading is facilitated by another apolipoprotein called a lipid transfer particle (LTP) (Canavoso et al., 2004). Both *Lpp* and *LTP* mutants are homozygous lethal (Palm et al., 2012). RNAi-mediated knockdown of either *Lpp* or *LTP* leads to intestinal lipid retention and reduced fat content in the fat body, ovaries, and brain, demonstrating the critical role *Lpp* and *LTP* play in lipid transport (Palm et al., 2012; Rodríguez-Vázquez et al., 2015).

Another small apolipoprotein called apolipophorin-III (ApoL-III) is found in the hemolymph of many insects. ApoL-III has the ability to switch between a lipid-free and a lipid-bound state and is, therefore, referred to as an exchangeable apolipoprotein (Weers and Ryan, 2003; Wientzek et al., 1994). Under conditions of high lipid demand, such as sustained flight in migratory locusts, DAGs

This is an open access article under the CC BY license (http://creativecommons.org/licenses/by/4.0/).

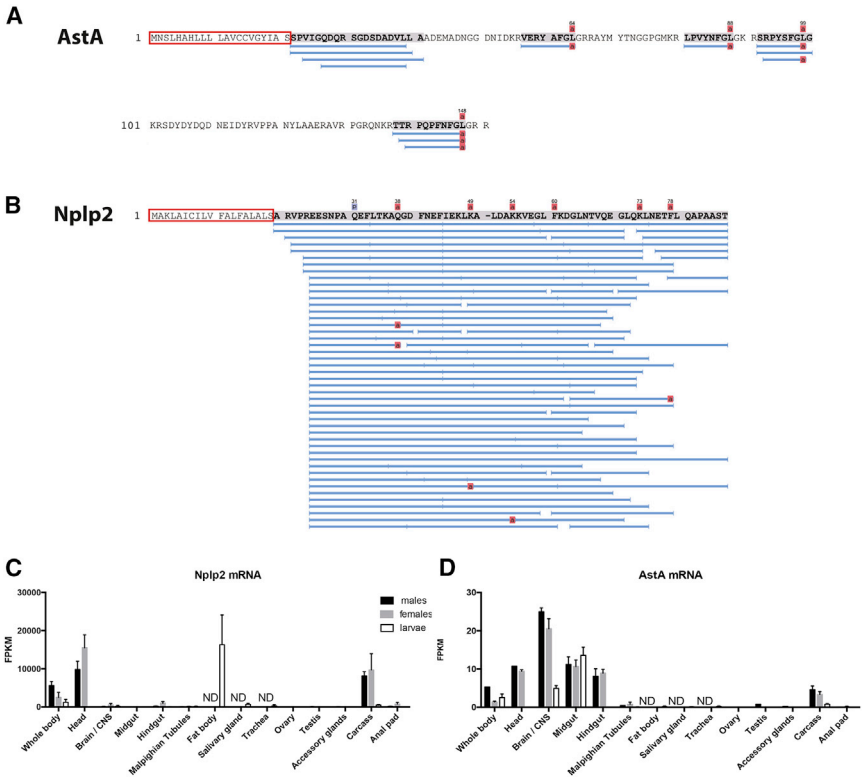

Figure 1. Nplp2 Is Not a Canonical Neuropeptide

(A and B) Mass spectrometry and *de novo* sequencing of a peptide-enriched third instar larval stage (L3) larval hemolymph fraction. Blue bars indicate the individual detected peptides derived from AstA (A) and Nplp2 (B). Colored squares represent amino acid modifications (a, amidation; p, pyro-glutamate), and red boxes highlight the signal peptide. See also Table S1.

(C and D) RNaseq data extracted from FlyAtlas2 showing *Nplp2* (C) and *AstA* (D) mRNA expression (expressed as fragments per kilobase million [FPKM]) in different tissues. *Nplp2* mRNA is mostly expressed in the head, brain, carcass, and larval fat body while *AstA* is mostly detected in the brain and gut. ND, not determined. Plotted are mean values ± SD.

are mobilized from fat body stores and transferred to HDLps (Arrese and Soulages, 2010). In this context, several ApoL-III molecules associate with HDLp and permit increased DAG loading onto the lipoprotein, transforming HDLp to LDLp (Ryan and Van der Horst, 2000). These lipid-rich particles are conveyed toward flight muscles where DAGs are hydrolyzed and ApoL-III is released. So far, no ApoL-III homolog has been identified in *Drosophila* (Palm et al., 2012).

In this study, we identified Nplp2 as an exchangeable apolipoprotein. We found that Nplp2 is required to resist heat stress, which suggests an unexpected role for lipoproteins in heat acclimation.

RESULTS

Nplp2 Is an Abundant Hemolymphatic Protein

Recent publications have described the proteome of the hemolymph under homeostatic conditions (Handke et al., 2013; Hartley et al., 2016; Zeng et al., 2015). The most abundant proteins were those involved in lipid and iron transport, as well as immunity. Surprisingly, one of the most abundant proteins was the putative neuropeptide Nplp2, a functionally uncharacterized, secreted peptide of 86 amino acids (10 kDa). Based on mass spectrometry analysis of the antennal lobe, Nplp2 was initially proposed to be a neuropeptide precursor (Baggerman et al., 2002, 2005), although several lines of evidence suggested otherwise. First, mature neuropeptides are generated by cleavage of a propeptide, usually at dibasic sites. However, the Nplp2-derived mature peptides described did not follow this rule. We set up an LC-MS analysis to detect mature neuropeptides in larval hemolymph. Using this strategy, we could identify several fully processed, C terminus-amidated neuropeptides previously described (Figure 1A; Table S1). For instance, analysis of Allatostatin A (AstA)-derived peptides identified only five short peptides, including four already described neuropeptides (Baggerman et al., 2002). In contrast to most neuropeptides, Nplp2-derived peptides covered the whole protein, with the exception of the signal peptide, and no enrichment for a processed peptide was found (Figure 1B). This result suggested that Nplp2-derived peptides were degradation products rather than processed neuropeptides. Moreover, Nplp2 was expressed at a very high level, which is unusual for neuropeptides that function as signaling molecules. It is worth noting that Nplp2 was one of the rare putative "neuropeptides" for which no cognate receptor is so far known. Finally, transcriptomic data from FlyAtlas2 showed that *Nplp2* did not have the expression profile expected for a canonical neuropeptide gene (Figures 1C and 1D). The gene is strongly expressed in fly heads and carcasses, notably the larval fat body, a storage organ with analogy to the mammalian liver. In contrast to many neuropeptides, Nplp2 was not expressed in the midgut. This proteomic analysis led us to suspect that Nplp2 was unlikely to be a neuropeptide precursor, a suspicion that was confirmed by the biochemical and genetic analysis described below.

Nplp2 Contains Amphipathic Alpha Helices and Binds to Lipids

The primary sequence of the Nplp2 protein is poorly conserved, even in the *melanogaster* species subgroup, and no significant homology outside the *Drosophila* genus was found using standard search algorithms. However, close inspection of the protein sequence revealed hydrophobic residues in every three to four amino acids (Figure 2A), a pattern reminiscent of amphipathic alpha helices (Segrest et al., 1990). Indeed, modeling of the protein using different methods (Phyre2, Swissmodel,

HHPred-Modeler; Zimmermann et al., 2017) consistently predicted a helix-turn-helix structure. Notably, all hydrophobic residues clustered on one side of each helix, reinforcing the idea that the protein had amphipathic helices (Figure 2A). Such structures are known to form helix bundles (Segrest et al., 1990). According to our model, the two helices are facing each other and are stabilized by hydrophobic interactions (Figure 2B). Such structures are found in lipid-binding proteins such as the insect exchangeable apolipoprotein ApoL-III (Wang et al., 2002).

ApoL-III structural properties and lipid-binding activity have been extensively characterized *in vitro* using dimyristoylphosphatidylcholine (DMPC) liposomes. ApoL-III undergoes a structural rearrangement upon phospholipid interaction and transforms spherical phospholipid liposomes into small, discoidal particles (Wientzek et al., 1994). We wondered if Nplp2 had similar properties. To test this, we produced recombinant *Drosophila* Nplp2 and *Manduca sexta* ApoL-III proteins, the latter being used as a positive control in the following assays. Far UV circular dichroism spectra revealed that both proteins harbor the typical signature of α-helical proteins, reinforcing the validity of our model (Figure 2C). Addition of DMPC liposomes consistently increased the circular dichroism (CD) signal for both proteins, with this increase being more pronounced in the case of Nplp2. The data suggest that the presence of liposomes stabilizes Nplp2 α helices. Indeed, the Nplp2 secondary structure was stabilized in the presence of liposomes, as evidenced by the important shift in melting temperature of the protein, while ApoL-III protein stability was not affected by liposome incubation (Figure 2D).

We then tested the ability of Nplp2 to bind lipids. First, Nplp2 protein was incubated with Bodipy-tagged fatty acids or phospholipids and submitted to native gel electrophoresis. Results showed that Nplp2 could efficiently bind free fatty acids and phospholipids (Figure S1A). Then, ApoL-III and Nplp2 were incubated with liposomes and submitted to native PAGE. Both ApoL-III and Nplp2 could efficiently bind liposomes (Figure 2E). We next measured their ability to transform liposomes into discoidal particles. Interestingly, both ApoL-III and Nplp2 efficiently transformed liposomes, while a control protein had no effect. Of note, at similar lipid:protein molar ratios, the Nplp2 transformation rate was faster than that of ApoL-III (Figure 2F). Liposomes incubated with ApoL-III or Nplp2 had remarkably comparable shapes and sizes (Figures 2G and 2H). Altogether, these results demonstrate that Nplp2 directly binds to liposomes and undergoes a structural rearrangement upon interaction with lipids. Based on these data, we conclude that Nplp2 forms ampipathic α helices and has lipid-binding properties.

Nplp2 Is a Lipid-Binding Protein and Is Found in the VLDL Fraction

The fact that Nplp2 is abundant in the hemolymph and shares similarities with ApoL-III, together with the absence of an identifiable ApoL-III ortholog in *Drosophila melanogaster*, raised the possibly that Nplp2 might function as an exchangeable apolipoprotein *in vivo*.

To test this hypothesis, we first undertook a biochemical approach by expressing an HA-tagged version of the protein *in vivo*. Nplp2-HA was detected in the hemolymph at its expected full-length size (16 kDa) confirming that the peptide is indeed secreted. No cleavage product of Nplp2-HA was detected (Figure 3A). Under native electrophoresis conditions, Nplp2-HA migrated at an apparent size of 60 kDa (Figure 3B). Similarly, a GFP-tagged overexpression construct of Nplp2 had a four times higher apparent molecular weight in native PAGE, as compared to denaturing conditions. These results strongly suggest that Nplp2 is engaged in a higher molecular weight complex or forms a multimer.

Since Nplp2 bound lipids, we expected to find it associated with lipoprotein particles in the hemolymph. To test this hypothesis, we separated larval hemolymph lipoprotein particles according to their density by isopycnic centrifugation. The major apolipoprotein, Lipophorin (Lpp), was mostly detected in the low-density lipoprotein (LDL) and very light density lipoprotein (VLDL) fractions of the gradient. In contrast, Nplp2 was found in the high-density lipoprotein (HDL) and the very light fractions (Figure 3C), suggesting that it exists in two distinct states: soluble or associated with VLDLs. Finally, in a detergent partitioning assay using larval hemolymph, Nplp2 was consistently found in both the soluble and the detergent fractions (Figure 3D). Thus, Nplp2 can be soluble in the hemolymph or segregate with VLDLs, a characteristic similar to that of exchangeable apolipoproteins such as insect ApoL-III or human ApoE (Chetty et al., 2003; Weers and Ryan, 2003). Collectively, our structural and biochemical studies reveal that Nplp2, despite its primary sequence divergence from ApoL-III found in other insects, may function as an exchangeable apolipoprotein in *Drosophila*.

The Nplp2 Tissue Localization Profile Is Similar to That of Lpp

In *Drosophila*, Lpp is mostly produced and secreted by the fat body (Arrese and Soulages, 2010; Palm et al., 2012). Lpp circulates in the hemolymph and transiently associates with tissues to deliver lipids. Lpp also localizes to the gut where it is loaded with lipids with the help of LTP. We wondered if Nplp2 also interacted with distant organs as described for the apolipoproteins Lpp and LTP. When specifically expressed in the fat body, Nplp2-HA localized intracellularly and at the plasma membrane of this organ with a pattern reminiscent of Lpp (Figure 4A) (Rodríguez-Vázquez et al., 2015). Fat-body-derived Nplp2 was also found in pericardial nephrocytes and in Garland cells at the gut anterior part (data not shown; Figure 4B, arrow head), which are involved in the removal of damaged proteins from the hemolymph. Importantly, Nplp2 was also detected in the anterior and posterior midgut (Figures 4B and 4C) in the two domains known to be involved in lipid absorption (Palm et al., 2012). Analysis of gut confocal sections revealed that Nplp2 was located in the extracellular space between the visceral muscle layer and the enterocytes, which is consistent with a function of an apolipoprotein extracting lipids (Figure 4D). Similar results were found with a transgenic line expressing an endogenously GFP-tagged version of the *Nplp2* locus (Sarov et al., 2016) (Figure S2). This localization of Nplp2 is very similar to that of Lpp in the larval gut ((Palm et al., 2012) and see below). Using a fly line carrying an endogenously GFP-tagged version of the *Lpp* locus (Sarov et al., 2016) and co-expressing Nplp2-HA, we found that the two proteins co-localized in the gut (Figure 4E) and the fat

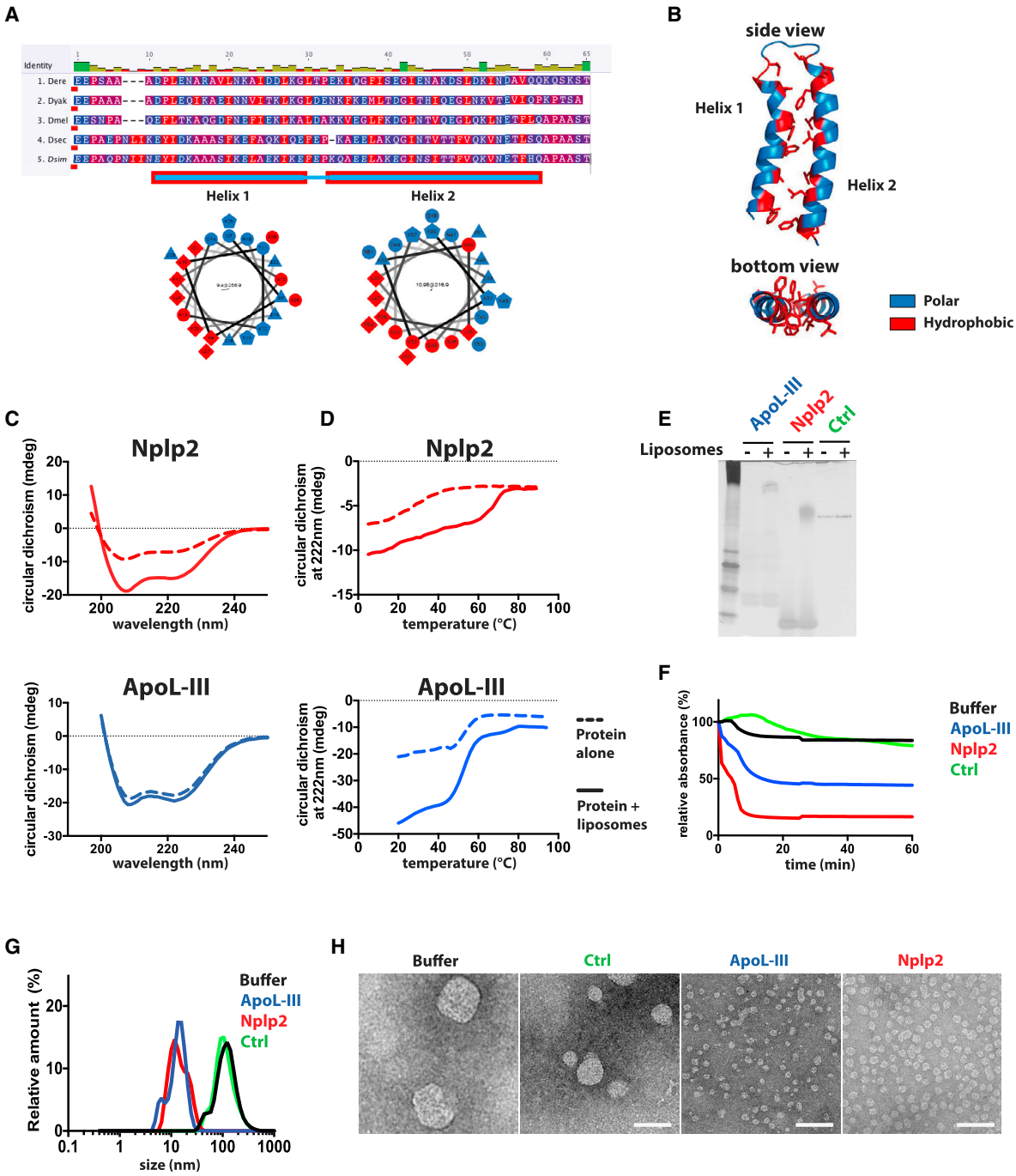

Figure 2. Nplp2 Carries Amphipathic Alpha Helices and Binds to Lipids

(A) Multiple alignment of Nplp2 protein sequences (without signal peptide). Hydrophobic residues (red) are regularly spaced and conserved across different *Drosophila* species. (Bottom) Helical wheel projections of predicted Nplp2 amphipathic helix 1 and 2. Red, hydrophobic residues; blue, polar residues.

(B) Side (top) and bottom (bottom) views of a model of Nplp2 structure using ApoL-III as a template. Hydrophobic residues from juxtaposed helices (in red) are facing each other.

(C) Representative experiments of circular dichroism spectra of Nplp2 (top) and ApoL-III (bottom) in solution (dashed line) or incubated with liposomes (solid line).

(D) Melting curves showing circular dichroism at 220 nm as a function of the temperature. Nplp2 melting temperature (top) increases if incubated with liposomes (solid line) while ApoL-III melting temperature (bottom) is not affected.

(E) Representative native gel of ApoL-III, Nplp2, and control protein incubated with or without liposomes. Proteins were stained by the silver staining method.

(F) Liposome clearance. ApoL-III (blue), Nplp2 (red), or control protein (green) were incubated with liposomes and absorbance decay was measured as a function of time. Data represent the pool of two independent experiments.

(legend continued on next page)

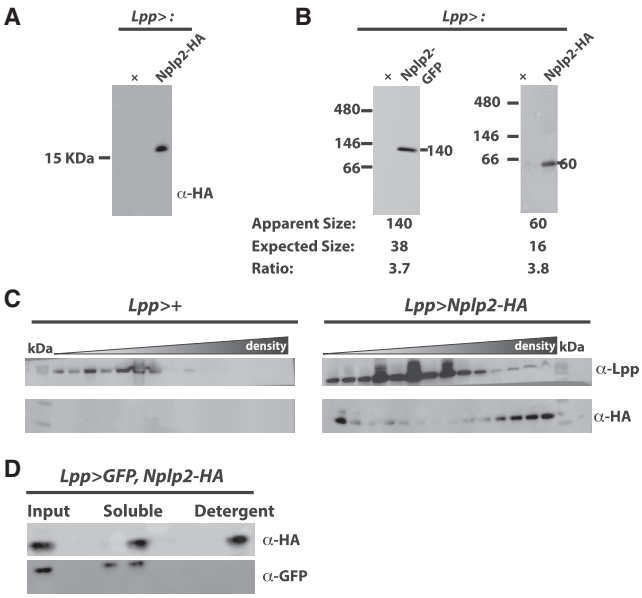

Figure 3. Nplp2 Segregates with Lipoproteins in the Hemolymph

(A) Anti-HA tag immunoblot of hemolymph from *Lpp > w*^{1118} or *Lpp>nplp2-HA* larvae run in denaturing conditions.

(B) Anti-GFP tag (left) or anti-HA tag (right) immunoblot of hemolymph from *Lpp > w*^{1118} and *Lpp>nplp2-GFP* (left) or *Lpp > w*^{1118} and *Lpp>Nplp2-HA* (right) larvae run in native conditions.

(C) Larval hemolymph from *Lpp > w*^{1118} (top) or Lpp > Nplp2-HA (bottom) was subjected to isopycnic centrifugation and fractions were immunoblotted with anti-Lpp (top) or anti-HA tag (bottom) antibodies.

(D) Tx-114 partitioning assay of larval hemolymph from *Lpp>GFP* or *Lpp > GFP, Nplp2-HA*. Soluble (aqueous) and detergent (hydrophobic) phases were analyzed by immunoblot to detect HA tag (top) or GFP (bottom). *Lpp>GFP* samples were loaded in duplicates. All experiments were repeated three times.

body (Figure 4A). Importantly, knocking down Lpp in the fat body abolished Nplp2 localization in the gut (Figure 4F). This last result showed that Nplp2 required Lpp for proper tissue addressing. Collectively, these data suggest that Nplp2 participates in lipid transport.

Silencing Nplp2 in the Fat Body Induces Intestinal Lipid Accumulation

Using CRISPR/Cas9 technology, we generated three independent fly lines carrying distinct deletions in the *Nplp2* gene that are all expected to be functional null alleles. Two of these mutants, *Nplp2*^{SK} and *Nplp2*^{154}, contain an indel causing a frameshift after the signal peptide sequence, while the third mutant, *Nplp2*^{156}, carries an 80-bp deletion leaving only 13 amino acids after the start codon (Figure S3A). Flies carrying any of these three mutations were homozygous viable and did not display any obvious morphological defects. Nevertheless, they showed substantial lethality during development with only 50% of eggs reaching adulthood (Figure S3B). Apolipoprotein knockdown leads to lipid retention in the larval gut (Palm et al., 2012). Since Nplp2 was found in the VLDL fraction, we tested whether a similar phenotype existed in *Nplp2*-deficient guts. Indeed, lipid droplet staining revealed a massive accumulation of neutral lipids in the larval gut of all three *Nplp2* mutants, notably in the cardia, the middle, and the posterior midgut. Lipid accumulation in the gut could be rescued by complementing the mutant strain with a wild-type copy of *Nplp2* (Figure 5A). Neutral lipid accumulation in the gut was also found in *Nplp2*-deficient adult flies, showing that Nplp2 likely functions in lipid mobilization in both larvae and adults (Figure S3C). Interestingly, neutral lipids accumulated in the same gut regions where Nplp2 was detected (Figure 4B). Furthermore, silencing *Nplp2* by RNAi, specifically in the fat body but not the gut, muscle, or brain, phenocopied the lipid accumulation found in *Nplp2*^{154} mutant guts (Figures 5B and S3D). These results indicate that fat-body-derived Nplp2 is required for intestinal lipid homeostasis and strongly suggest a function in lipid transport. Quantification of intestinal levels of both DAGs and TAGs confirmed a 3–5-fold increase in neutral lipid content in the gut of all three *Nplp2* mutant larvae, as compared to the wild type (Figures 5C, S3E, and S7A). In contrast to the Lpp or LTP knockdown phenotype, phospholipid and sterol levels were not significantly higher in the gut of *Nplp2*-deficient larvae and adults (Figures S3F and S3G), suggesting a specific role of the protein in neutral lipid transport. To confirm these data, we performed a lipidomic analysis of control and *Nplp2*^{154} mutant larval guts. TAGs but not phospholipid levels were massively increased (up to 200 fold) in *Nplp2*-deficient guts (Table S2).

Nplp2 Deficiency Reduces Lipid Transport and Storage in the Fat Body

The intestinal steatosis observed in *Nplp2* mutants could be a consequence of either increased lipid synthesis in enterocytes or reduced lipid transport from the gut to peripheral tissues. To distinguish between these two options, we first fed larvae with sucrose only. If intestinal *de novo* lipogenesis was increased in mutants, the amounts of gut lipids should be similar between normal and sucrose-fed *Nplp2* mutant larvae. In contrast, the accumulation of lipid in *Nplp2* mutants was reduced in larvae fed with sucrose (Figure S4A). Moreover, feeding larvae with a fluorescently labeled fatty acid resulted in a stronger signal in the anterior and posterior midgut of *Nplp2*-deficient larvae compared to wild-type ones, confirming that, in mutants, dietary lipids are not efficiently translocated to the hemolymph (Figure 5D). These results show that lipid accumulation in *Nplp2*-deficient larvae is likely to be a consequence of reduced transport. We next subjected control and mutant hemolymph to a density gradient. As expected, the Lpp apparent density was higher in mutant hemolymph, as compared to the control, a phenotype partially rescued by reintroducing a wild-type copy of *Nplp2* in the mutant background (Figure 5E). To definitively demonstrate that Nplp2 participates in intestinal lipid

(G) Size of lipid:protein complexes from samples described in (F) was measured by dynamic light scattering. Data shown are means of three independent experiments.

(H) Transmission electron micrographs of DMPC liposomes incubated with PBS, control protein, ApoL-III, or Nplp2. Liposome-protein complexes were incubated for 20 h at room temperature. See also Figure S1.

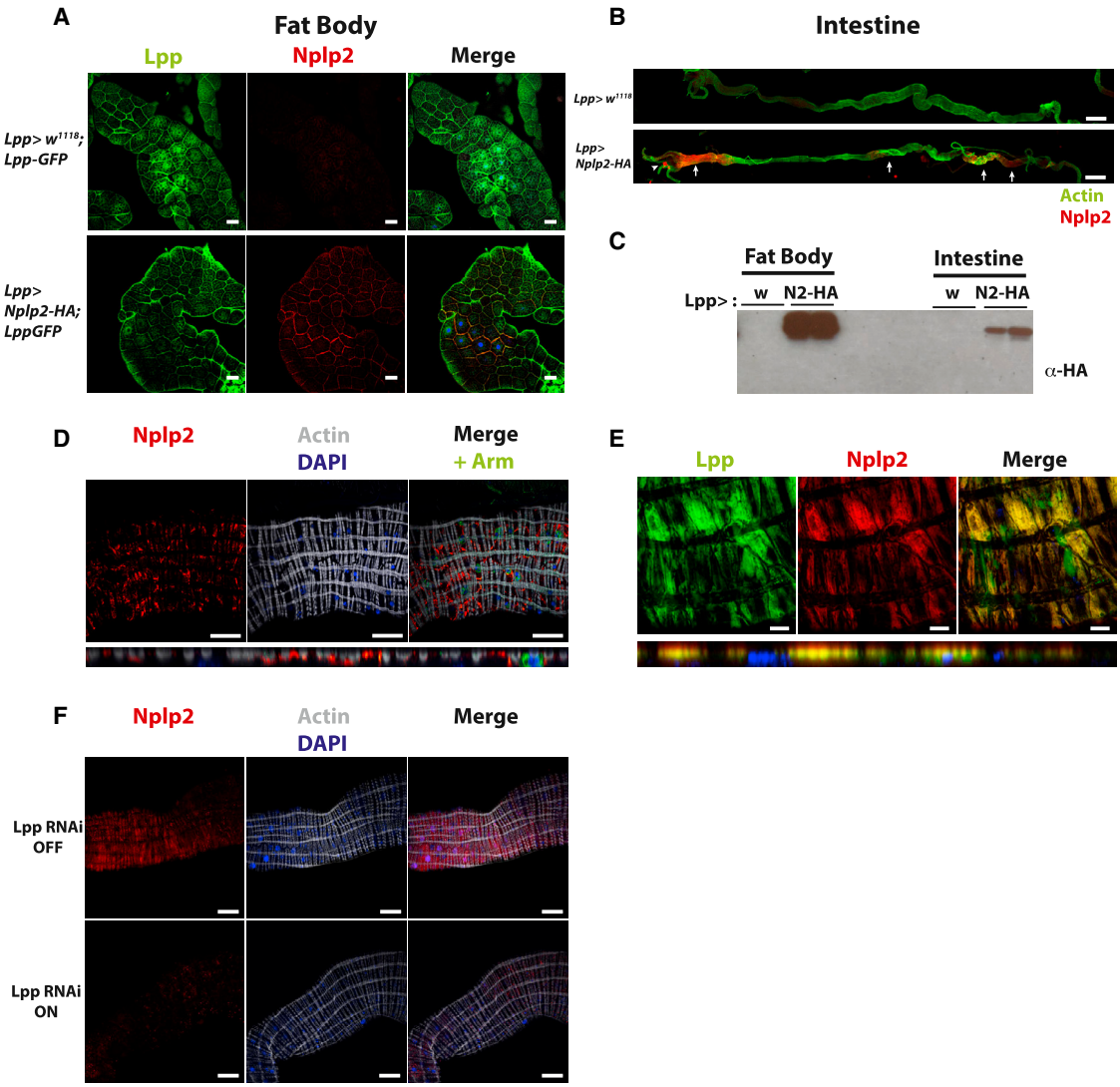

Figure 4. Fat-Body-Derived Nplp2 Localizes to the Gut Close to Lpp

(A) Confocal imaging of larval fat bodies from *LppGFP*, *Lpp > w*^{1118} (top) or *LppGFP, Lpp > Nplp2-HA* (bottom). Tissues were co-stained with anti-GFP (green, left) and anti-HA (red, middle).

(B–D) Fat-body-derived Nplp2 is found in the gut. (B) Intestines from *Lpp > w*^{1118} (top) or *Lpp>Nplp2-HA* (bottom) larvae were stained with phalloidin (green) and anti-HA tag antibody (red). Nplp2 is found in Garland cells (arrowhead) and in the anterior and posterior midgut (arrows). (C) Fat bodies and guts from the same larvae as in (B) were subjected to anti-HA immunoblot (two biological replicates). (D) Confocal images of *Lpp>Nplp2-HA* larval guts stained with anti-HA (red), anti-armadillo (Arm, progenitor cell marker, green), and phalloidin (gray). (Bottom) An orthogonal view of successive confocal z stacks.

(E) Confocal images of larval guts (same genotypes as in A) stained with anti-GFP (green) and anti-HA tag (red) antibodies. (Bottom) An orthogonal view of successive confocal images. Arrows indicate the extracellular space between enterocytes and visceral muscles.

(F) Confocal images of hsFlp;;*Lpp > ;Lpp RNAi; Nplp2-HA* larval guts stained with anti-HA (red), phalloidin, and DAPI (gray and blue, respectively). (Bottom) Lpp RNAi was induced by several heat shocks. Scale bar: 20 μm. See also Figure S2.

loading onto Lpp, we perform an *ex vivo* assay. Hemolymph from lipid-starved larvae was incubated with explanted guts and subsequently subjected to density gradient. In the presence of wild-type guts, Lpp in hemolymph of wild-type animals was loaded with lipids. Lipid loading was reduced when hemolymph of *Nplp2* mutants was incubated with wild-type guts (Figure S4B), showing that a circulating factor absent in *Nplp2*-deficient hemolymph controls VLDLs formation. Strikingly, the addition of recombinant Nplp2 to hemolymph from wild-type larvae further enhanced Lpp lipid loading *ex vivo* (Figure 5F). Altogether, these data demonstrate a role of Nplp2 in Lpp loading and intestinal lipid mobilization.

Retention of dietary lipids in the gut is expected to alter lipid distribution to other tissues (Palm et al., 2012). Consequently, we monitored the amount of TAG in the larval fat body and the hemolymph of *Nplp2* mutants. *Nplp2*^{SK} mutant and wild-type larvae had comparable lipid amounts in the hemolymph and the fat body (Figures 5G, 5H, and S6A–S6C). Similarly, the

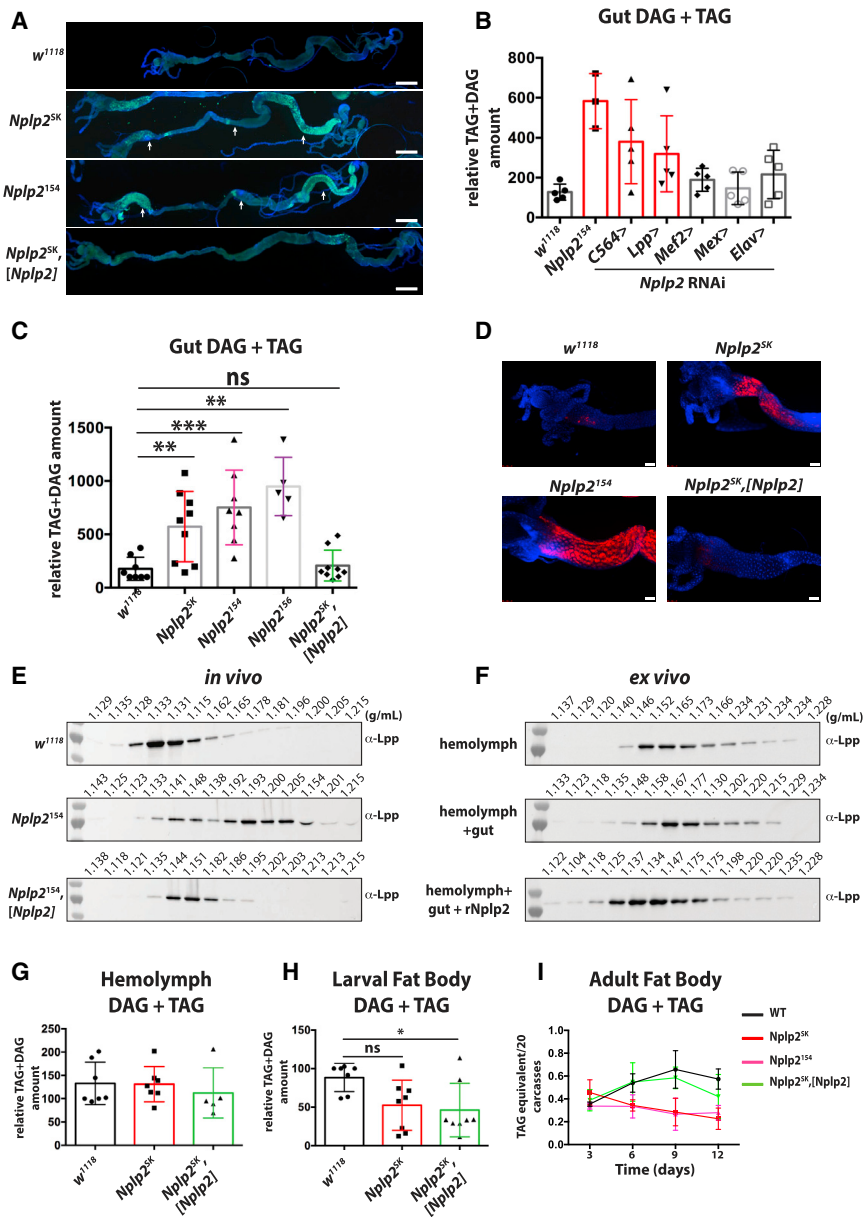

Figure 5. Nplp2-Deficient Larvae Show Impaired Lipid Transport from the Gut

(A) Bodipy staining (green and DAPI in blue) of wild-type and nplp2 deficient larval guts shows a neutral lipid accumulation in anterior, middle, and posterior mutant midguts (arrows).

(B) TAG+DAG quantification of guts from *UAS-Nplp2 RNAi* line crossed with different Gal4 driver lines. Values from at least two independent experiments are represented as mean ± SD. Red bars indicate a significant difference ($p < 0.05$).

(C, G, and H) Measurement of DAG+TAG in larval guts (C), hemolymph (G), and fat bodies (H). Wild-type values are depicted in black, $Nplp2^{SK}$ in red, and $nplp2^{SK}$,[*nplp2*] in green. (**$p < 0.005$; ***$p < 0.0005$; ns, non significant; Mann-Whitney test was used.)

(D) Representative pictures of anterior midgut from larvae fed Bodipy-C12-FL (red). Tissues were fixed, stained with DAPI (blue), and imaged immediately. Mutant flies accumulate fluorescent lipids in their anterior midgut. Similar results were observed in the posterior midgut (not shown). Scale bar: 10 μm (n = 2).

(E and F) representative immunoblots against Lpp after isopycnic gradient of larval hemolymph. (E) Hemolymph extracted from larvae was immediately centrifuged to monitor the endogenous lipoprotein density. (F) Hemolymph from lipid-starved larvae was co-cultured with guts dissected from larvae fed a standard food prior to centrifugation to monitor the intestinal lipid transfer to Lpp. Blots are representative of three independent experiments.

(I) Quantification of TAG+DAG in wild-type (black), $Nplp2^{SK}$ (red), $Nplp2^{154}$ (pink), and $nplp2^{SK}$,[*nplp2*] (green) adult male flies of different ages (*$p < 0.05$; ****$p < 0.00005$, two-way ANOVA and Tukey's post test, n = 3). TAG+DAG contents were normalized to protein amounts. Plotted are mean values of at least three independent experiments ± SD. Each symbol on histograms represents a biological replicate. See also Figures S3, S4, S6, and S7.

amounts of sterol were only marginally altered in mutant hemolymph and fat bodies (Figures S4C and S4D). This suggests that in our laboratory conditions *Nplp2* mutant larvae are able to compensate the neutral lipid transport defect to produce normal fat body stores.

We however noticed a higher variability in the amount of lipid stores in $Nplp2^{SK}$ mutant larvae compared to the wild-type ones. The presence of larvae with low fat stores could explain the partial developmental lethality observed with *Nplp2* null mutants. We reasoned that a difference could be more striking in adults, where flight increases energy consumption (Berrigan and Partridge, 1997). Three-day-old *Nplp2* males had fat body stores similar to wild-type animals. However, fat levels were decreasing with age in *Nplp2*-deficient males, while wild-type and $Nplp2^{SK}$,*[Nplp2]* rescued adults increased their lipid stores (Figure 5I). This result shows that Nplp2 is required for the maintenance of lipid storage in adult flies. Altogether, these data demonstrate that Nplp2 contributes to lipid redistribution from the gut, as well as to fat body storage, and further confirms that Nplp2 is an apolipoprotein.

Nplp2 Deficiency Is Associated with Abnormal Lipoprotein Homeostasis

In rodents and humans, ApoE binds to VLDL particles and enhances their clearance from plasma through LDL receptor-mediated endocytosis (Feingold and Grunfeld, 2000). Additionally, ApoE enhances VLDL production in the endoplasmic reticulum of hepatocytes and their subsequent secretion to the plasma

(Sundaram and Yao, 2012). Due to this double function, *ApoE* deficiency provokes dyslipidemia accompanied by a dyslipoproteinemia, caused by a delayed clearance of chylomicrons and VLDL remnant particles (Breslow, 1996). In *Drosophila*, knockdown of Lpp or LTP in the larval fat body also provokes intestinal steatosis (Lee et al., 2017; Palm et al., 2012; Rodríguez-Vázquez et al., 2015). As Nplp2 co-localizes with Lpp, we wondered if the levels of Lpp and LTP apolipoproteins were normal in *Nplp2*-deficient larvae. *Lpp* and *LTP* mRNA abundance was increased in *Nplp2* mutant larvae compared to controls (Figure 6A). To monitor protein levels, we generated wild-type and *Nplp2* mutant fly lines expressing tagged versions of Lpp (Sarov et al., 2016) and LTP (Rodríguez-Vázquez et al., 2015). Both Lpp and LTP proteins were found intracellularly and at the plasma membrane of the fat body of the control larvae (Figure 6B), as previously reported for LTP (Rodríguez-Vázquez et al., 2015). Surprisingly, while the number of apolipoprotein mRNAs tended to be higher in *Nplp2* mutants, the number of both proteins appeared to be almost identical in the control and *Nplp2*-deficient fat bodies (Figure 6C). In line with this finding, immunoblot quantification of Lpp and LTP showed no significant increase of both proteins in mutant fat bodies (Figures 6F and 6G). This suggests that Lpp and LTP are post-transcriptionally regulated in the absence of Nplp2 either by increased protein turnover or by increased reallocation of Lpp and LTP from the site of production. In support of the latter, the amount of Lpp in both the anterior and the posterior midgut was strongly increased in *Nplp2*-deficient mutants (Figures 6D, 6E, and S5A). Importantly, Lpp accumulated in the same gut compartments where Nplp2 was found (Figure 4B) and where lipids accumulated in *Nplp2*-deficient larvae (Figure 5A). Immunoblot analysis confirmed the accumulation of Lpp observed in *Nplp2*-deficient guts (Figure 6H). In contrast, immunostaining suggested that LTP was reduced in these gut regions (Figures 6D and 6E). Moreover, immunoblot analysis showed that Lpp was more abundant in the hemolymph of *Nplp2*-deficient larvae (Figure 6I), while the amount of LTP was decreased (Figure 6J). An altered localization of Lpp and LTP was also found in larval anterior midguts and in adult guts (Figures S5B and S5C). Altogether, these data show that *Nplp2* larvae and adults present a dyslipoproteinemia, an abnormal distribution of apolipoproteins characterized by reduced levels of gut LTP and mislocalization of Lpp. The gut lipid retention observed in *Nplp2*-deficient animals can be explained by the absence of LTP in the intestine leading to insufficient lipid loading onto Lpp. Therefore, we conclude that Nplp2 affects Lpp and LTP protein levels in the circulation and in the gut to optimize neutral lipid uptake from the gut.

Nplp2 Participates in Thermal Acclimation

All the results described so far indicate that Nplp2 is an apolipoprotein involved in lipid redistribution from the gut. While *apolpp* or *apoltp* mutants are lethal at the larval stage, *Nplp2*-deficient flies only show a partial developmental lethality and can give rise to viable adults. Additionally, the high variability in fat storage observed in *Nplp2* mutant larvae suggests that Nplp2 may be sensitive to additional environmental factors. In *Drosophila*, thermal stress rapidly depletes glycogen and TAG stores in the fat body (Klepsatel et al., 2016; Sarup et al., 2016). After thermal challenge, flies need several days to regenerate their initial lipid stores, a process that likely relies on the increased transport of dietary lipids by lipoproteins. We therefore hypothesized that Nplp2 might have a critical role in promoting optimal fat store maintenance after exposure to heat stress. Consistent with this notion, we observed that $Nplp2^{SK}$ mutants had severely reduced eclosion rates compared to wild-type animals when raised at 29°C (Figure S3B). To avoid any interference with development, we further analyzed the role of Nplp2 in heat resistance at the adult stage. We first monitored the levels of Nplp2 protein at various temperatures using flies carrying an endogenously *GFP*-tagged *Nplp2* gene (Sarov et al., 2016). Figure 7A shows that the level of *Nplp2-GFP* protein increased after exposure to heat but not to cold. We then subjected *Nplp2* and wild-type flies to an acute heat stress for 45 min at 38°C and assessed fat body TAG content 3 days later. At that time, lipid stores in wild-type flies were similar to those of unchallenged flies. In sharp contrast, lipid stores were significantly reduced in *Nplp2* mutant flies (Figure 7B). Thus, the Nplp2 apolipoprotein plays a critical role in maintaining fat body stores from gut lipids after heat stress.

We then assessed the role of Nplp2 in the resistance to chronic heat stress. For this, we compared the survival of wild-type and *Nplp2*-deficient flies continuously kept at 32°C. While *Nplp2* mutants exhibited a reduced lifespan at 25°C as compared to their appropriate controls, this difference was further amplified when flies were raised at 32°C (Figures 7C and 7D). After 7 days at 32°C, the fat-body-neutral lipid content was reduced in both wild-type and mutant animals. This decrease was, however, more pronounced in *Nplp2*-deficient flies compared to wild type (Figures 7E and 7F). The increased lethality of *Nplp2* flies raised at 32°C is likely due to their inability to efficiently extract and transport dietary lipids. To test this notion, we analyzed the survival of flies at 32°C raised on a hypocaloric medium that reduces nutrient uptake. The survival of wild-type animals at 32°C was reduced, emphasizing that flies need nutritious food to cope with elevated environmental temperatures (Figure 7G). On a low-calorie diet, *Nplp2*-deficient flies died at a rate similar to their wild-type counterparts. Collectively, this suggests that *Nplp2*-deficient animals exposed to a chronic heat stress are in a "starved" condition even when raised on a nutritious diet.

Altogether our data show that Nplp2 is required for optimal lipid storage in adult fat body. Under high nutrient demands such as heat stress, the absence of Nplp2 leads to lipid store depletion and adult mortality. Thus, Nplp2 is an important apolipoprotein of *Drosophila*, with a critical role in the adaptation to elevated environmental temperatures.

DISCUSSION

In this study, we investigated the function of Nplp2, an abundant hemolymphatic protein that was initially thought to be a neuropeptide. Instead, our data led us to conclude that Nplp2 functions as an exchangeable apolipoprotein. *Nplp2*-deficient flies show intestinal steatosis and dyslipoproteinemia. While *Nplp2* mutants are still viable, Nplp2 is required to sustain fat stores in adult flies. Importantly, Nplp2 is induced upon thermal stress

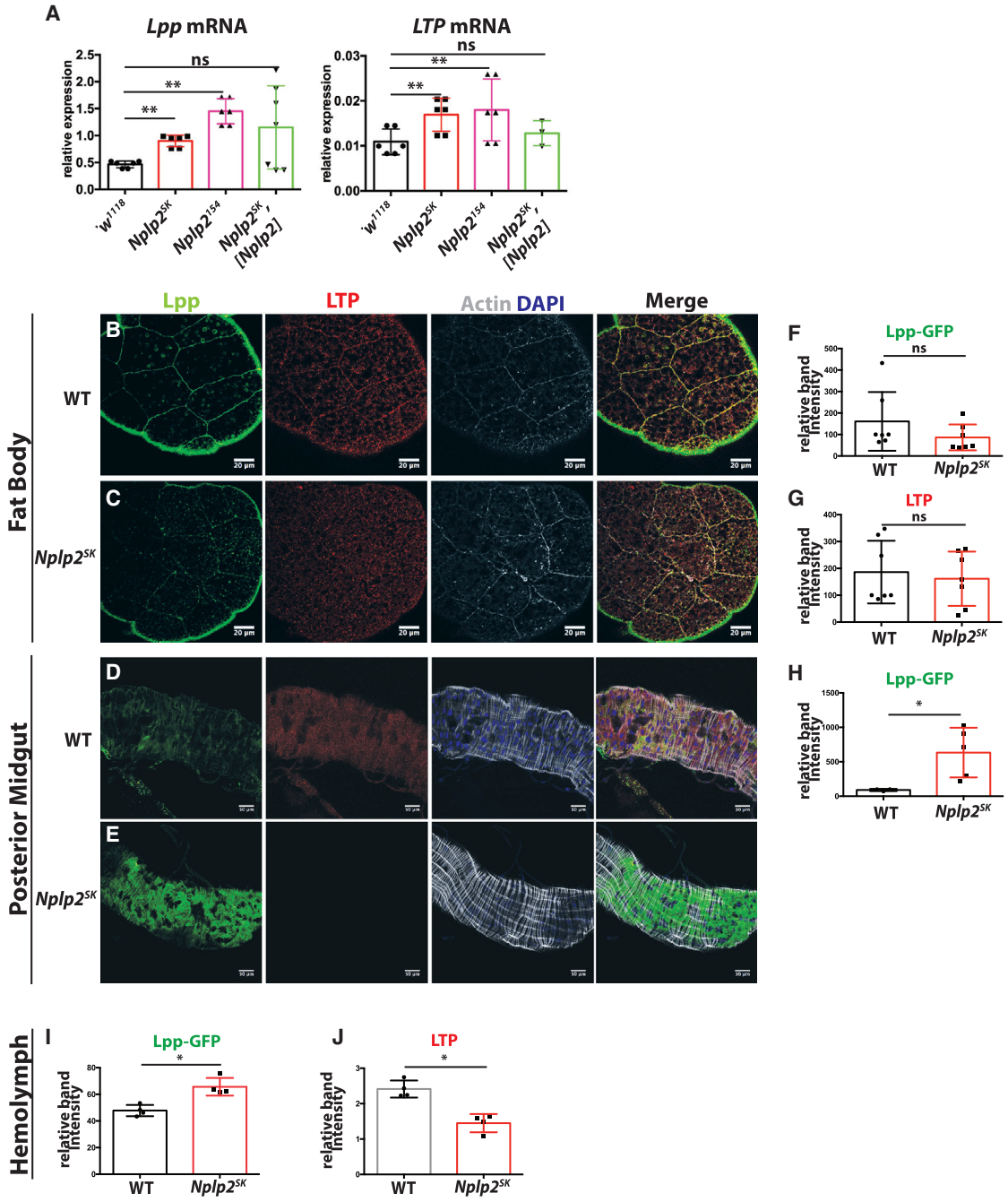

Figure 6. Nplp2-Deficient Larvae Have a Dyslipoproteinemia

(A) RT-qPCR analysis of Lpp (left) and LTP (right) transcripts of wild-type, *nplp2*^{SK}, *nplp2*^{154}, and nplp2^{SK},[*nplp2*] whole larvae.

(B–E) Representative immunostainings of *LppGFP*, *LTP-V5* and *LppGFP*, *LTP-V5*, *and nplp2*^{SK} larval fat bodies (B and C, respectively) and posterior midgut (D and E, respectively). Tissues were stained with anti-GFP (Lpp, green) and anti-V5 (LTP, red) antibodies and counterstained with phalloidin (actin, gray).

(F, H, and I) Tissues from the same genotype as in (B)–(E) were analyzed by immunoblot. LppGFP was quantified in fat body (F), gut (H), and hemolymph (I).

(G and J) LTP-V5 was detected in fat body (G) and hemolymph (J). Values from three independent experiments are plotted as mean ± SD. Each symbol on histograms represents a biological replicate (*$p < 0.05$; **$p < 0.005$; ns, non significant; Mann-Whitney test was used) Scale bar: 20 μm. See also Figure S5.

and contributes to metabolic adaptation to heat. We propose that Nplp2 associates with triglyceride-rich LDLp under homeostatic conditions and under high-energy demand (e.g., heat stress) to maintain optimal fat stores. Below, we discuss our findings in the light of insect lipid transport and optimization of this machinery to stressful conditions.

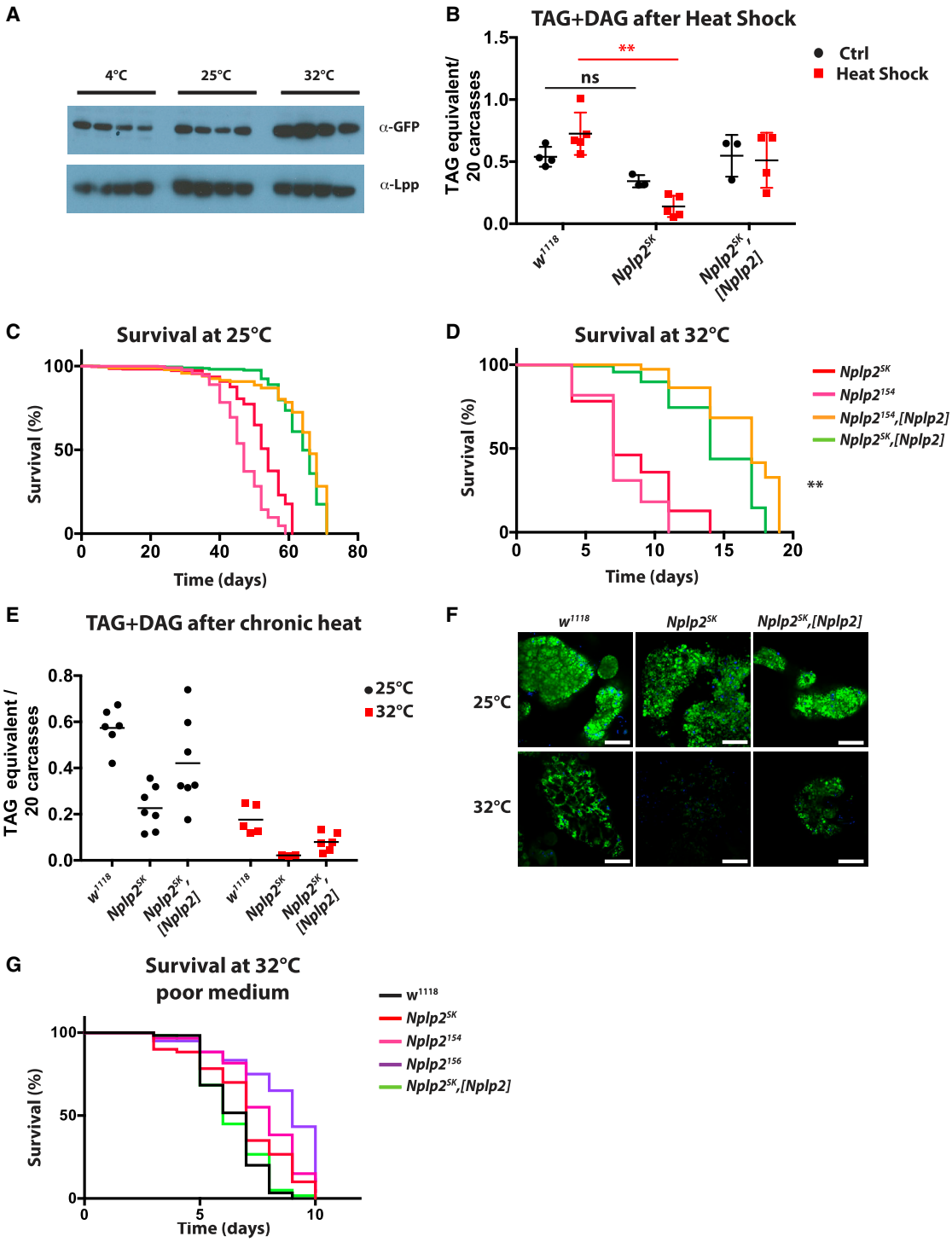

Figure 7. Nplp2 Is Required for Optimal TAG Storage in Adults

(A) Immunoblot analysis of Nplp2-GFP adult flies kept at 4°C, 25°C, or 32°C for 18 h. Anti-GFP (top) was used to detect Nplp2 and anti-Lpp (bottom) was used as a loading control.

(B) Three-day-old male flies were heat shocked for 45 min at 38°C (red bars) or not (black bars) and then kept at 25°C. After 3 days, fat body TAGs were quantified; n = 4 (*p < 0.05).

(legend continued on next page)

Low Evolutionary Conservation of ApoL-III among Insects

In *Drosophila*, lipid transport is mediated by the large, non-exchangeable apolipoproteins Lpp and LTP. These proteins were readily identified by sequence homology prediction based on apolipoproteins identified in other insects, and functional analysis has confirmed their role in *Drosophila* lipid metabolism (Palm et al., 2012). Biochemical studies of other insects pointed to the existence of an additional exchangeable apolipoprotein, ApoL-III, which promotes LDLp formation and lipid mobilization (Ryan and van der Horst, 2000). The *Drosophila* genome annotation did not reveal any homolog to ApoL-III. Therefore, it was proposed that this class of apolipoprotein was absent from *Drosophila* (Palm et al., 2012). Our analysis reveals that Nplp2 behaves as an exchangeable apolipoprotein. While there is no sequence homology between ApoL-III and Nplp2, both proteins have amphipathic α helices, bind lipids, and are involved in neutral lipid transport by increasing lipid cargo on lipoprotein particles. These proteins have however different biophysical properties regarding helical content and liposome transformation capacity. Moreover, ApoL-III forms five amphipathic helix bundles while Nplp2 has only two predicted helices. The latter could multimerize to form a bundle similar to ApoL-III. However, a truncated ApoL-III harboring only three helices had lipid binding ability comparable to a full-length protein, suggesting that Nplp2 could also be active as a monomer (Dettloff et al., 2001). Therefore, it is tempting to speculate that Nplp2 is a functional analog of ApoL-III in *Drosophila*. Interestingly, ApoL-III protein structures from two distantly related insects, a locust and a lepidopteran, revealed remarkable structural conservation despite poor amino-acid identity (Breiter et al., 1991; Wang et al., 2002). These studies suggest that the selective pressure to maintain the ApoL-III sequence at the gene level is weaker than for other apolipoproteins. We hypothesize that this relaxed constraint on the DNA sequence is due to the fact that ApoL-III is not as essential for lipid transport as Lpp, as exchangeable apolipoproteins merely optimize lipid transport in certain contexts. This would explain the rapid evolution of ApoL-III at the sequence level to maximize lipid transport efficiency in contexts specific to given insect species, such as migratory flight or environmental stresses. Nplp2 increases lipid cargo per lipoprotein, as ApoL-III does in other insects. Nplp2 overexpression leads to a reduction in fat body TAG content, suggesting that it might also be involved in fat body lipid mobilization (Figure S6). However, Nplp2 has non-redundant functions in intestinal lipid loading, a function never shown for ApoL-III. It cannot be excluded that our analysis allowed us to uncover an uncharacterized function for ApoL-III, which may apply to other insects. Alternatively, although Nplp2 and ApoL-III are both exchangeable lipoproteins, they may be involved in different physiological contexts: lipid assimilation and mobilization, respectively. If this is true, this difference is an example of the evolutionary specialization of the lipid transport system. Future studies should better characterize the role of Nplp2 and its relation with other insect apolipoproteins such as ApoL-III.

Nplp2 Affects Lipoprotein Homeostasis and Lipid Transport

The use of *Nplp2*-deficient flies confirms its role in lipid homeostasis. In contrast with other apolipoprotein mutants, *Nplp2*-deficient viable flies can be obtained under laboratory conditions. Nevertheless, Nplp2 function is required to build optimal lipid stores in both larvae and adults. Reduced levels of the essential apolipoproteins Lpp and LTP have been associated with the accumulation of lipids in the intestine. Consistent with Nplp2 functioning as an apolipoprotein, *Nplp2* mutant flies also show intestinal lipid retention proving that Nplp2 is indispensable for efficient lipid redistribution from the gut. Our study further shows that Nplp2 is produced in the fat body and localizes at the plasma membrane and intracellularly. Nplp2 segregates with LDLp in circulation and is attached to the enterocytes along with Lpp. Two non-mutually exclusive mechanisms could explain the accumulation of lipids in *Nplp2* mutants. In the absence of Nplp2, fewer lipids are loaded on Lpp, provoking an intestinal steatosis. However, the effect could also be indirect, as we found that *Nplp2* flies have lower intestinal LTP levels and increased Lpp protein amounts. Thus, the accumulation of lipid in the intestine of Nplp2 mutants could be a secondary consequence of defects in LTP and Lpp. According to this hypothesis, Nplp2 would not only directly contribute to lipid transport but also regulate lipoprotein homeostasis. Disentangling these two functions is challenging given the complex reciprocal interactions between lipoproteins. Nplp2 could have a dual role by allowing the formation of LDLp in the hemolymph and by controlling the appropriate localization of apolipoproteins. Palm et al. (2012) have shown that LTP requires active endocytosis by enterocytes to be properly located and active. Therefore, Nplp2 could be required for LTP endocytosis, in a fashion similar to the function of mammalian ApoE. In humans, VLDL-bound ApoE interacts with LDL receptors to promote lipid particle endocytosis by hepatocytes (Feingold and Grunfeld, 2000). Nplp2 and LTP could also interact with an unknown receptor, possibly the Lpp receptor LpR2, which is expressed in the midgut (Parra-Peralbo and Culi, 2011), to allow LTP endocytosis into enterocytes. The increased Lpp and LTP levels in *Nplp2* mutants, which are also detected at the transcript level, could be a compensatory mechanism to maximize lipid extraction in the absence of Nplp2 and to maintain a normolipemia. On the other hand, dyslipoproteinemia has often been associated with dyslipidemia and could be a secondary consequence of the altered lipid content of lipoproteins. Although our results suggest that Nplp2 is likely to control lipid uptake by properly addressing LTP to the gut, further

(C, D, and G) Lifespans of $Nplp2^{154}$ (pink), $Nplp2^{SK}$ (red), $Nplp2^{154}$,[*nplp2*] (orange), and $nplp2^{SK}$,[*nplp2*] (green) females kept on standard food at 25°C (C) or at 32°C (D) or on a hypocaloric medium at 32°C (G). Results shown are representative of at least three independent experiments containing two to three cohorts each (****$p < 0.00005$; log-rank test).

(E) Fat body TAG+DAG quantitation of WT and mutant male flies kept for 9 days at 25°C (black) or 32°C (red); n = 7 (**$p < 0.005$; *$p < 0.05$; ns, non significant; Mann-Whitney test was used).

(F) Representative confocal micrographs of male carcasses stained with Bodipy (green) and DAPI (blue). Scale bar: 20 μm.

investigation is needed to understand the molecular mechanisms involved.

Nplp2 Optimizes Lipid Uptake under Stressful Conditions

ApoL-III function in insects has been described during sustained flight of migratory locusts, a process that requires a massive energy supply (Arrese and Soulages, 2010). In the wild, *Drosophila* are not expected to perform long flights and therefore rather depend on carbohydrates as an energy source. Therefore, Nplp2 must have a different role in *Drosophila* physiology. Our study shows that Nplp2 has non-redundant functions related to lipid transport and contributes to lipid stores and survival at normal temperatures. While *Nplp2*-deficient flies have reduced fat stores in normal conditions, the role of Nplp2 in lipid store formation appears to be critical in mature adults under heat stress. While responses to stress have been the focus of intense research (e.g., heat shock response), rare studies have focused on lipid metabolism adaptation to stress. Several mechanisms could explain the increased susceptibility of *Nplp2* mutants to heat stress. First, Nplp2 could scavenge damaged lipids. A similar mechanism was already described for another inducible lipoprotein, Glial Lazarillo (GLaz) (Sanchez et al., 2006). Interestingly, loss of this lipid-binding protein led to reduced energy stores and increased susceptibility to oxidative stress. More recently, Liu et al., (2017) published research showing that overexpressing human ApoE can rescue Glaz deficiency, suggesting that ApoE and GLaz have overlapping functions in the brain. As Nplp2 and ApoE share structural homology, Nplp2 could exert a protective role during heat stress by scavenging oxidized lipids.

A second hypothesis is that Nplp2 could be involved in the transport of certain lipids that are specifically required for heat stress acclimation. Previous studies have shown that larval food composition affects adult thermal stress tolerance, showing that dietary macromolecules can modulate cytoprotection (Andersen et al., 2010). This is also emphasized by the fact that flies change their dietary preferences when the ambient temperature drops. Indeed, food-derived lipids were shown to be required to maximize survival by maintaining appropriate membrane fluidity at lower temperatures (Brankatschk et al., 2018). Our study shows that Nplp2 is critical for lipid storage at high temperature. However, our lipidomic data show that mostly TAGs are retained in *Nplp2*-deficient guts. This suggests that the role of Nplp2 is mainly confined to enhancing TAG transport, an essential adaptive process. Consequently, we propose that Nplp2 promotes heat stress tolerance by supplying tissues with TAGs to fuel the heat acclimation. In ectotherms, increased ambient temperature results in higher metabolic rates (Orr, 1925). As a consequence, nutrient uptake and assimilation have to increase. Higher temperature also results in cellular damage and the activation of a heat stress response, which relies on the synthesis of ATP-dependent molecular chaperones in order to restore homeostasis. These processes require an important amount of energy and the reallocation of energetic resources to cope with the stress. Upon stress exposure, organisms reduce anabolic processes such as growth, energy storage, or reproduction to redirect their metabolic fluxes toward cytoprotection, resulting in a transient reduction in fitness (Sokolova, 2013). Metabolic rewiring upon stress is not only observed in insects but also in mammals, suggesting that it is a generic adaptation mechanism (Sokolova, 2013). Here, we have identified an exchangeable, heat-inducible apolipoprotein that is required for thermal acclimation. Our results suggest that induction of a lipid uptake and transport system is part of an integrated cytoprotective response. Thus, besides energy reallocation, increased nutrient assimilation is also a strategy to increase survival while maintaining fitness during heat stress. As ApoL-III was also reported to be induced by heat stress in *Galleria mellonella* (Verty-porokh et al., 2015), the role of Nplp2 and ApoL-III is likely to be conserved across different insect species. In conclusion, by identifying an exchangeable apolipoprotein, our study fills an important gap in our understanding of the lipid transport machinery in *Drosophila*. Moreover, it also reveals the importance of lipid metabolism adaptation to heat stress, a notion that should be taken into consideration when studying ectotherm species acclimation to global warming.

STAR★METHODS

Detailed methods are provided in the online version of this paper and include the following:

- KEY RESOURCES TABLE
- CONTACT FOR REAGENT AND RESOURCE SHARING
- EXPERIMENTAL MODEL AND SUBJECT DETAILS
  - *Drosophila* stocks and treatments
- METHOD DETAILS
  - Recombinant protein production
  - Fluorescent lipid binding assay
  - Liposomes transformation assay
  - Electron microscopy
  - Dynamic light scattering
  - Circular Dichroism
  - Generation of Nplp2 deficient flies
  - Generation of transgenic flies
  - Quantitative PCR
  - Histology and immunostaining
  - Hemolymph proteins separation
  - Western blotting
  - Peptide fraction preparation
  - LC-MS/MS analysis
  - Lipids measurements
  - Lipidomics
- QUANTIFICATION AND STATISTICAL ANALYSIS
  - Bioinformatics and structural prediction
  - Statistical analyses

SUPPLEMENTAL INFORMATION

Supplemental Information can be found online at https://doi.org/10.1016/j.celrep.2019.03.074.

ACKNOWLEDGMENTS

We thank Marc Moniatte for his expertise in proteomics, Ana de Busturia for fruitful discussions, and Anass Chiki for help with liposome preparation. We also thank Ronald Kühnlein for a critical reading of the manuscript. We are

also very grateful to Suzanne Eaton (Max Planck Institute, Dresden), Joaquim Culi (Universidad Pablo de Olavide, Sevilla), and Jose Soulages (Oklahoma State University) for providing fly stocks, antibodies, and plasmids. We are thankful to Bloomington and VDRC stock centers for fly stocks. This work was supported by the Swiss National Fund (SNSF; 3100A0-12079/1).

AUTHOR CONTRIBUTIONS

S.R., J.-P.B., and J.P. conducted the experiments. S.K. generated the Nplp2^{SK} mutants. S.R. and B.L. designed the experiments and wrote the paper.

DECLARATION OF INTERESTS

The authors declare no competing interests.

Received: June 20, 2018
Revised: February 11, 2019
Accepted: March 19, 2019
Published: April 16, 2019

REFERENCES

Andersen, L.H., Kristensen, T.N., Loeschcke, V., Toft, S., and Mayntz, D. (2010). Protein and carbohydrate composition of larval food affects tolerance to thermal stress and desiccation in adult Drosophila melanogaster. J. Insect Physiol. *56*, 336–340.

Arrese, E.L., and Soulages, J.L. (2010). Insect fat body: energy, metabolism, and regulation. Annu. Rev. Entomol. *55*, 207–225.

Baggerman, G., Cerstiaens, A., De Loof, A., and Schoofs, L. (2002). Peptidomics of the larval *Drosophila melanogaster* central nervous system. J. Biol. Chem. *277*, 40368–40374.

Baggerman, G., Boonen, K., Verleyen, P., De Loof, A., and Schoofs, L. (2005). Peptidomic analysis of the larval Drosophila melanogaster central nervous system by two-dimensional capillary liquid chromatography quadrupole time-of-flight mass spectrometry. J. Mass Spectrom. *40*, 250–260.

Barry, W.E., and Thummel, C.S. (2016). The Drosophila HNF4 nuclear receptor promotes glucose-stimulated insulin secretion and mitochondrial function in adults. Elife *5*, e11183.

Berrigan, D., and Partridge, L. (1997). Influence of temperature and activity on the metabolic rate of adult Drosophila melanogaster. Comp. Biochem. Physiol. A: Physiol. *118*, 1301–1307.

Bligh, E.G., and Dyer, W.J. (1959). A rapid method of total lipid extraction and purification. Can. J. Biochem. Physiol. *37*, 911–917.

Brankatschk, M., and Eaton, S. (2010). Lipoprotein Particles Cross the Blood-Brain Barrier in Drosophila. J Neurosci. *30*, 10441–10447.

Brankatschk, M., Gutmann, T., Knittelfelder, O., Palladini, A., Prince, E., Grzybek, M., Brankatschk, B., Shevchenko, A., Coskun, Ü., and Eaton, S. (2018). A temperature-dependent switch in feeding preference improves Drosophila development and survival in the cold. Dev. Cell *46*, 781–793.

Breiter, D.R., Kanost, M.R., Benning, M.M., Wesenberg, G., Law, J.H., Wells, M.A., Rayment, I., and Holden, H.M. (1991). Molecular structure of an apolipoprotein determined at 2.5-A resolution. Biochemistry *30*, 603–608.

Breslow, J.L. (1996). Mouse models of atherosclerosis. Science *272*, 685–688.

Canavoso, L.E., Yun, H.K., Jouni, Z.E., and Wells, M.A. (2004). Lipid transfer particle mediates the delivery of diacylglycerol from lipophorin to fat body in larval *Manduca sexta*. J. Lipid Res. *45*, 456–465.

Chetty, P.S., Arrese, E.L., Rodriguez, V., and Soulages, J.L. (2003). Role of helices and loops in the ability of apolipophorin-III to interact with native lipoproteins and form discoidal lipoprotein complexes. Biochemistry *42*, 15061–15067.

Dettloff, M., Weers, P.M., Niere, M., Kay, C.M., Ryan, R.O., and Wiesner, A. (2001). An N-terminal three-helix fragment of the exchangeable insect apolipoprotein apolipophorin III conserves the lipid binding properties of wild-type protein. Biochemistry *40*, 3150–3157.

Esteves, A., Knoll-Gellida, A., Canclini, L., Silvarrey, M.C., André, M., and Babin, P.J. (2016). Fatty acid binding proteins have the potential to channel dietary fatty acids into enterocyte nuclei. J. Lipid Res. *57*, 219–232.

Feingold, K.R., and Grunfeld, C. (2000). Introduction to lipids and lipoproteins. In Endotext, K.R. Feingold, B. Anawalt, and A. Boyce, et al., eds. (MDText.com). https://www.ncbi.nlm.nih.gov/books/NBK305896/.

Fründ, J., Zieger, S.L., and Tscharntke, T. (2013). Response diversity of wild bees to overwintering temperatures. Oecologia *173*, 1639–1648.

Handke, B., Poernbacher, I., Goetze, S., Ahrens, C.H., Omasits, U., Marty, F., Simigdala, N., Meyer, I., Wollscheid, B., Brunner, E., et al. (2013). The hemolymph proteome of fed and starved Drosophila larvae. PLoS ONE *8*, e67208–e67210.

Hartler, J., Trötzmüller, M., Chitraju, C., Spener, F., Köfeler, H.C., and Thallinger, G.G. (2011). Lipid Data Analyzer: unattended identification and quantitation of lipids in LC-MS data. Bioinformatics *27*, 572–577.

Hartley, P.S., Motamedchaboki, K., Bodmer, R., and Ocorr, K. (2016). SPARC-dependent cardiomyopathy in Drosophila. Circ. Cardiovasc. Genet. *9*, 119–129.

IPCC. (2014). Climate Change 2014: Synthesis Report. Contribution of Working Groups I, II and III to the Fifth Assessment Report of the Intergovernmental Panel on Climate Change. https://www.ipcc.ch/site/assets/uploads/2018/05/SYR_AR5_FINAL_full_wcover.pdf.

Jessen, F., and Wulff, T. (2015). Triton X-114 cloud point extraction to subfractionate blood plasma proteins for two-dimensional gel electrophoresis. Anal. Biochem. *485*, 11–17.

Jevanandam, N., Goh, A.G.R., and Corlett, R.T. (2013). Climate warming and the potential extinction of fig wasps, the obligate pollinators of figs. Biol. Lett. *9*, 20130041.

Klepsatel, P., Gáliková, M., Xu, Y., and Kühnlein, R.P. (2016). Thermal stress depletes energy reserves in Drosophila. Sci. Rep. *6*, 33667.

Klok, C.J., and Chown, S.L. (1997). Critical thermal limits, temperature tolerance and water balance of a sub-Antarctic caterpillar, Pringleophaga marioni (Lepidoptera: Tineidae). J Insect Physiol. *43*, 685–694.

Kondo, S., and Ueda, R. (2013). Highly improved gene targeting by germline-specific Cas9 expression in *Drosophila*. Genetics *195*, 715–721.

Lee, J.-S., Kwak, S.-J., Kim, J., Kim, A.-K., Noh, H.M., Kim, J.-S., and Yu, K. (2014). RNA-guided genome editing in Drosophila with the purified Cas9 protein. G3: Genes Genomes Genet. *4*, 1291–1295.

Lee, S., Bao, H., Ishikawa, Z., Wang, W., and Lim, H.-Y. (2017). Cardiomyocyte regulation of systemic lipid metabolism by the apolipoprotein B-containing lipoproteins in Drosophila. PLoS Genet. *13*, e1006555.

Liu, L., MacKenzie, K.R., Putluri, N., Maletić-Savatić, M., and Bellen, H.J. (2017). The glia-neuron lactate shuttle and elevated ROS promote lipid synthesis in neurons and lipid droplet accumulation in glia via APOE/D. Cell Metab. *26*, 719–737.

Martinet, B., Lecocq, T., Smet, J., and Rasmont, P. (2015). A protocol to assess insect resistance to heat waves, applied to bumblebees (Bombus Latreille, 1802). PLoS ONE *10*, e0118591.

Nyamukondiwa, C., Weldon, C.W., Chown, S.L., le Roux, P.C., and Terblanche, J.S. (2013). Thermal biology, population fluctuations and implications of temperature extremes for the management of two globally significant insect pests. J. Insect Physiol. *59*, 1199–1211.

Orr, P.R. (1925). Critical thermal increments for oxygen consumption of an insect, Drosophila melanogaster. J. Gen. Physiol. *7*, 731–734.

Palm, W., Sampaio, J.L., Brankatschk, M., Carvalho, M., Mahmoud, A., Shevchenko, A., and Eaton, S. (2012). Lipoproteins in Drosophila melanogaster–assembly, function, and influence on tissue lipid composition. PLoS Genet. *8*, e1002828.

Parra-Peralbo, E., and Culi, J. (2011). Drosophila lipophorin receptors mediate the uptake of neutral lipids in oocytes and imaginal disc cells by an endocytosis-independent mechanism. PLoS Genet. *7*, e1001297.

Pleiner, T., Bates, M., and Görlich, D. (2018). A toolbox of anti–mouse and anti–rabbit IgG secondary nanobodies. J Cell Biol. *217*, 1143.

Rappsilber, J., Mann, M., and Ishihama, Y. (2007). Protocol for micro-purification, enrichment, pre-fractionation and storage of peptides for proteomics using StageTips. Nat. Protoc. *2*, 1896–1906.

Rodríguez-Vázquez, M., Vaquero, D., Parra-Peralbo, E., Mejía-Morales, J.E., and Culi, J. (2015). Drosophila lipophorin receptors recruit the lipoprotein LTP to the plasma membrane to mediate lipid uptake. PLoS Genet. *11*, e1005356.

Ryan, R.O., and van der Horst, D.J. (2000). Lipid transport biochemistry and its role in energy production. Annu. Rev. Entomol. *45*, 233–260.

Ryuda, M., Tabuchi, M., Matsumoto, H., Matsumura, T., Ochiai, M., and Hayakawa, Y. (2018). A gene-driven recovery mechanism: *Drosophila* larvae increase feeding activity for post-stress weight recovery. Arch. Insect Biochem. Physiol. *97*, e21440.

Saibil, H. (2013). Chaperone machines for protein folding, unfolding and disaggregation. Nat. Rev. Mol. Cell Biol. *14*, 630–642.

Sanchez, D., López-Arias, B., Torroja, L., Canal, I., Wang, X., Bastiani, M.J., and Ganfornina, M.D. (2006). Loss of glial lazarillo, a homolog of apolipoprotein D, reduces lifespan and stress resistance in Drosophila. Curr. Biol. *16*, 680–686.

Sarov, M., Barz, C., Jambor, H., Hein, M.Y., Schmied, C., Suchold, D., Stender, B., Janosch, S., K J, V.V., Krishnan, R.T., et al. (2016). A genome-wide resource for the analysis of protein localisation in Drosophila. eLife *5*, e12068.

Sarup, P., Petersen, S.M.M., Nielsen, N.C., Loeschcke, V., and Malmendal, A. (2016). Mild heat treatments induce long-term changes in metabolites associated with energy metabolism in Drosophila melanogaster. Biogerontology *17*, 873–882.

Schindelin, J., Arganda-Carreras, I., Frise, E., Kaynig, V., Longair, M., Pietzsch, T., Preibisch, S., Rueden, C., Saalfeld, S., Schmid, B., et al. (2012). Fiji: an open-source platform for biological-image analysis. Nat Methods *9*, 676.

Segrest, J.P., De Loof, H., Dohlman, J.G., Brouillette, C.G., and Anantharamaiah, G.M. (1990). Amphipathic helix motif: classes and properties. Proteins *8*, 103–117.

Sokolova, I.M. (2013). Energy-limited tolerance to stress as a conceptual framework to integrate the effects of multiple stressors. Integr. Comp. Biol. *53*, 597–608.

Sundaram, M., and Yao, Z. (2012). Intrahepatic role of exchangeable apolipoproteins in lipoprotein assembly and secretion. Arterioscler. Thromb. Vasc. Biol. *32*, 1073–1078.

Verleyen, P., Baggerman, G., D'Hertog, W., Vierstraete, E., Husson, S.J., and Schoofs, L. (2006). Identification of new immune induced molecules in the haemolymph of Drosophila melanogaster by 2D-nanoLC MS/MS. J. Insect Physiol. *52*, 379–388.

Vertyporokh, L., Taszłow, P., Samorek-Pieróg, M., and Wojda, I. (2015). Short-term heat shock affects the course of immune response in Galleria mellonella naturally infected with the entomopathogenic fungus Beauveria bassiana. J. Invertebr. Pathol. *130*, 42–51.

Wang, J., Sykes, B.D., and Ryan, R.O. (2002). Structural basis for the conformational adaptability of apolipophorin III, a helix-bundle exchangeable apolipoprotein. Proc. Natl. Acad. Sci. USA *99*, 1188–1193.

Weers, P.M.M., and Ryan, R.O. (2003). Apolipophorin III: a lipid-triggered molecular switch. Insect Biochem. Mol. Biol. *33*, 1249–1260.

Wientzek, M., Kay, C.M., Oikawa, K., and Ryan, R.O. (1994). Binding of insect apolipophorin III to dimyristoylphosphatidylcholine vesicles. Evidence for a conformational change. J. Biol. Chem. *269*, 4605–4612.

Zeng, Q., Smith, D.J., and Shippy, S.A. (2015). Proteomic analysis of individual fruit fly hemolymph. J. Chromatogr. B Analyt. Technol. Biomed. Life Sci. *981-982*, 33–39.

Zimmermann, L., Stephens, A., Nam, S.-Z., Rau, D., Kübler, J., Lozajic, M., Gabler, F., Söding, J., Lupas, A.N., and Alva, V. (2017). A completely reimplemented MPI bioinformatics toolkit with a new HHpred server at its core. J. Mol. Biol. *430*, 2237–2243.

STAR★METHODS

KEY RESOURCES TABLE

REAGENT or RESOURCE	SOURCE	IDENTIFIER
Antibodies		
chicken anti-GFP	Abcam	Cat# ab13970; RRID: AB_300798
Mouse monoclonal anti-V5 tag	Thermo Fischer Scientific	Cat# R960-25; RRID:AB_2556564
Rat monoclonal anti-HA tag	Roche	Cat# 3F10; RRID:AB_2314622
Goat anti-Chicken IgY (H+L) Secondary Antibody, Alexa Fluor 488	Thermo Fischer Scientific	Cat# A11039; RRID: AB_2534096
Goat anti-Rat IgG (H+L) Cross-Adsorbed Secondary Antibody, Alexa Fluor 555	Thermo Fischer Scientific	Cat# A21434; RRID: AB_2535855
Goat anti-Mouse IgG (H+L) Highly Cross-Adsorbed Secondary Antibody, Alexa Fluor 555	Thermo Fischer Scientific	Cat# A21424; RRID: AB_141780
mouse anti-Myc tag antibody	Millipore	Cat# MABE282; RRID:AB_11213164
Peroxidase-AffiniPure Donkey Anti-Rat IgG (H+L)	Jackson ImmunoResearch Labs	Cat# 712-035-150; RRID:AB_2340638
Peroxidase-AffiniPure Donkey Anti-Rabbit IgG (H+L)	Jackson ImmunoResearch Labs	Cat# 711-035-152; RRID:AB_10015282
Peroxidase-AffiniPure Goat Anti-Rat IgG (H+L)	Jackson ImmunoResearch Labs	Cat# 112-035-003; RRID:AB_2338128
Chemicals, Peptides, and Recombinant Proteins		
GeneArt Cas9 Platinum	Thermo Fischer Scientific	B25640
Synthetic Nplp2 protein	Thermo Fischer Scientific	N/A
Recombinant Nplp2	This study	N/A
Recombinant Manduca sexta ApoL-III	This study	N/A
T7 endonuclease	New England Biolabs	M0302S
DMPC	Avanti polar lipids	850345
4',6-Diamidino-2-phenylindole dihydrochloride (DAPI)	Sigma	Cat# D9542; CAS: 28718-90-3
BodipyTM 558/568-C12	Life Technologies	D3835
BodipyTM-500/510-C11-HPC	Life Technologies	D3793
BodipyTM 493/503	Life Technologies	D3922
Alexa647 Phalloidin	Life Technologies	Thermo Fisher Scientific Cat# A22287; RRID:AB_2620155
complete protease inhibitor	Sigma	11697498001
phenylmethylsulfonyl fluoride	Sigma	P7626
Potassium Bromide	Sigma	P3691
Triton-X-114 (10% solution)	Thermo Scientific	28332
Control peptide	GenicBio	N/A
N-Phenylthiourea	Sigma	222909
1,2-didodecanoyl-sn-glycero-3-phosphocholine	Avanti Polar Lipids (Alabaster, AL, USA)	850325C
1-heptadecanoyl-2-myristoleoyl-sn-glycero-3-phosphocholine	Avanti Polar Lipids (Alabaster, AL, USA)	850325C
1-heptadecanoyl-2-myristoleoyl-sn-glycero-3-phosphoethanolamine	Avanti Polar Lipids (Alabaster, AL, USA)	LM1104
1-heptadecanoyl-2-myristoleoyl-sn-glycero-3-phospho-(1'-myo-inositol)	Avanti Polar Lipids (Alabaster, AL, USA)	LM1504
1-heptadecanoyl-2-myristoleoyl-sn-glycero-3-phospho-L-serine	Avanti Polar Lipids (Alabaster, AL, USA)	LM1304
N-(dodecanoyl)-sphing-4-enine-1-phosphocholine	Avanti Polar Lipids (Alabaster, AL, USA)	LM2312
N-(heptadecanoyl)-sphing-4-enine;	Avanti Polar Lipids (Alabaster, AL, USA)	860517
D-glucosyl-β-1,1'N-octanoyl-D-erythro-sphingosine	Avanti Polar Lipids (Alabaster, AL, USA)	860540

(*Continued on next page*)

Continued

REAGENT or RESOURCE	SOURCE	IDENTIFIER
sn-(3-tetradecanoyl-2-hydroxy)-glycerol-1-phospho-sn-3′-(1’-tetradecanoyl-2′-hydroxy)-glycerol	Avanti Polar Lipids (Alabaster, AL, USA)	857131
Bis-[2-(9Z-octadecenoyl)-3-lyso-sn-glycero]-1-phosphate	Avanti Polar Lipids (Alabaster, AL, USA)	857131
1,2-ditetradecanoyl-sn-glycero-3-phospho-(1’-sn-glycerol)	Avanti Polar Lipids (Alabaster, AL, USA)	840033
1,2-di-(9E-octadecenoyl)-sn-glycero-3-phospho-(1’-sn-glycerol)	Avanti Polar Lipids (Alabaster, AL, USA)	840033
1,2,3-Trioctanoyl-sn-glycerol	Sigma (St. Louis, MO, USA)	N/A
1,2,3-Tridecanoyl-sn-glycerol	Sigma (St. Louis, MO, USA)	N/A
1,2,3-Tridodecanoyl-sn-glycerol	Sigma (St. Louis, MO, USA)	N/A
1,2,3-Tritetradecanoyl-sn-glycerol	Sigma (St. Louis, MO, USA)	N/A
1,2,3-trihexadecanoyl-sn-glycerol	Sigma (St. Louis, MO, USA)	N/A
1,3-Dioctadecanoyl-sn-glycerol	Sigma (St. Louis, MO, USA)	800855
(18:1(9Z)/18:1(9Z)/0:0)1,2-di-(9Z-octadecenoyl)-sn-glycerol	Sigma (St. Louis, MO, USA)	800811
1,2-Dihexadecanoyl-sn-glycerol	Sigma (St. Louis, MO, USA)	D0138
Experimental Models: Organisms/Strains		
w1118;;Nplp2SK	This study	N/A
w1118;;Nplp2154	This study	N/A
w1118;;Nplp2156	This study	N/A
w1118;;BAC[Nplp2]	This study	N/A
w1118;UAS-Nplp2-HA	This study	N/A
w1118;UAS-Nplp2-GFP	This study	N/A
w1118;;Nplp2-GFP	Schnoerrer	VDRC 318263
w1118;; Lpp-GFP	Schnoerrer	VDRC 318255
w1118;;BAC[LTP-myc-V5]	Rodriguez-Vasquez &Culi	N/A
Lpp-gal4	Brankatschk and Eaton, 2010	N/A
MHC-gal4	BDSC	BDSC Cat# 38464; RRID:BDSC_38464
Mex-gal4	Barry and Thummel, 2016	N/A
Elav-gal4	BDSC#8765	N/A
Actin-gal4	BDSC	BDSC Cat# 25374; RRID:BDSC_25374
C564-gal4	BDSC	BDSC Cat# 6982; RRID:BDSC_6982
FAS IR	VDRC	FlyBase Cat# FBst0457934; RRID:FlyBase_FBst0457934
Nplp2 IR	BDSC	BDSC Cat# 54041; RRID:BDSC_54041
Oligonucleotides		
Rp49F: TCTGCATGAGCAGGACCTC	Microsynth	N/A
Rp49R: ATCGGTTACGGATCGAACAA	Microsynth	N/A
Lpp F: CACCAGTAAAGGGGCTCTCA	Microsynth	N/A
Lpp R: CCAGCCACCGTTATTAAGGA	Microsynth	N/A
LTP F: GGCGCAGAGCTTCTTTAGTG	Microsynth	N/A
LTP R: CGCTGATCGAAGGTCATGTA	Microsynth	N/A
gRNA ebony: TCTTCGAGGAGCAGCAGCTGCGG	Microsynth	N/A
gRNA 154: GTCCGCCCGCGTCCCCCGTGAGG	Microsynth	N/A
gRNA 156: GCTCCGTAGCTCTAAACGCTCGG	Microsynth	N/A
Recombinant DNA		
pPWH-Nplp2	This study	N/A
pTWG-Nplp2	This study	N/A

(*Continued on next page*)

Continued

REAGENT or RESOURCE	SOURCE	IDENTIFIER
p[ACMAN]-attB-Nplp2	This study	N/A
pET32b-Nplp2	This study	N/A
pET32b-ApoL-III	This study, based on Chetty et al., 2003	N/A
pTP1172,	Pleiner et al., 2018	Addgene #104161
Software and Algorithms		
Fiji	Schindelin et al., 2012	http://fiji.sc/
Prism 5	GraphPad	https://www.graphpad.com/scientific-software/prism/
Peaks Studio 8.5	(BSI, Canada)	N/A
Lipid Data Analyzer II	Hartler et al., 2011	N/A
Geneious	Geneious	N/A
HHPred	Zimmermann et al., 2017	https://toolkit.tuebingen.mpg.de
PyMol	https://pymol.org/2/	https://pymol.org/2/

CONTACT FOR REAGENT AND RESOURCE SHARING

Further information and requests for resources and reagents should be directed to and will be fulfilled by the Lead Contact, B. Lemaitre (Bruno.lemaitre@epfl.ch).

EXPERIMENTAL MODEL AND SUBJECT DETAILS

Drosophila stocks and treatments

Drosophila stocks were maintained at 25°C on a standard fly medium made of 6% cornmeal, 6% yeast, 0.62% agar, 0.1% fruit juice, that was supplemented with 10.6g/L Moldex and 4.9ml/L propionic acid. Unless indicated otherwise, w^{1118} flies were used as a wild-type control. 30 males per tube were heat-shocked 45min at 38°C and immediately returned to 25°C. For survival experiments, 20 female flies were kept at 25°C or 32°C and survival was counted daily. In some experiments, flies were kept on a low-calorie food containing 20% nutrient from a regular medium, with 1.2% cornmeal, 1.2% yeast, 0.62% agar supplemented with 0.98ml/L propionic acid.

METHOD DETAILS

Recombinant protein production

Drosophila Nplp2 and Manduca sexta APoL-III were cloned into pET32b vector by Gibson assembly with an N-terminal thioredoxin-tag, His-tag and a Tobacco Etch Virus (TEV) protease cleavage site, and expressed overnight at 18°C by addition of 0.2 mM isopropylthio-β-galactoside in *E. coli rosetta-gami B (DE3)* strain (Merck). Cells were lysed by sonication in 20 mM Tris pH 8.5, 300 mM NaCl, 10 mM imidazole, one tablet of protease inhibitor cocktail (Complete, EDTA-free, Roche), benzonase nuclease (25U/ml lysis buffer, Novagen) at 4°C, and purified on Ni-NTA agarose (QIAGEN). The tags were removed with TEV protease by overnight dialysis in 20 mM Tris pH 8.5 and 300 mM NaCl buffer, followed by "reverse" Ni-NTA purification. Nplp2 and ApoL-III were further purified by size-exclusion chromatography on a HiLoad superdex75 10/30 GL column (GE healthcare) and concentrated to mg/ml in 20 mM Tris pH 8.5 and 300 mM NaCl buffer. Protein purity was verified on SDS gel (NUPAGE 10%–20% Tricine gel) and estimated at > 95%. A nanobody against the mouse immunoglobulin G kappa chain was used a control protein (pTP1172, Addgene #104161). The protein was produced according to the supplier's instruction.

Fluorescent lipid binding assay

Lipid binding assay was done as described (Esteves et al., 2016). 10 μL of 147 μM Nplp2 synthetic protein (Life Technologies) or 10 μL of 27 μM Fatty acid-free Bovine Serum albumin (Sigma) were mixed in PBS with 10 μL of 2 μM Bodipy™ 558/568-C_{12} or 10 μL of 20 μM Bodipy™-500/510-C_{11}-HPC (Life Technologies), incubated 5min at room temperature and subjected to native polyacrylamide gel electrophoresis (Life Technologies) in the dark for 1h30. Fluorescence was recorded on a Fusion FX7 gel imager with appropriate filters and total protein staining using InstantBlue™ (Expedeon) was done afterward.

Liposomes transformation assay

1mg of DMPC dissolved in chloroform was evaporated under N2 stream and the lipid film was lyophilized overnight. Lipids were vigorously mixed with 500ul PBS and sonicated in a waterbath for 15 min at 37°C. Liposomes were then extruded through a

0.2 μm pore size membrane (Avanti). Liposomes and proteins were mixed at a 1mg/ml and 61 μM final concentration, respectively (31:1 lipid:protein molar ratio), and decay in absorbance at 325nm was immediately recorded in a Tecan infinite-200 equipped with a temperature controller set at 24°C. Complexes were then incubated overnight and subjected to native gel electrophoresis (Novex 4%–12% Tris-Glycine gel, Thermo Scientific) followed by silver staining (Pierce).

Electron microscopy

15 μL of 2mg/mL DMPC Liposomes were incubated with 15 μL 87 μM Nplp2, ApoL-III or control protein, or 174 μM Nplp2 synthetic peptide (EESNPAQEFLTKAQGDFNEFIEKLKALDAKKVEGLFKDGLNTVQEGLQKLNETFLQAPAAST, ThermoFisher) or control peptide (QFHVERPGRTVDVGNGGFYIQRG, GenicBio) and incubated for 20h at room temperature. Samples were subsequently diluted 25 times in PBS and pipetted on the carbon-coated grid (400 mesh copper Grids, Canemco-Marivac) for 2 min after glow discharge treatment, the grid was washed with distilled water, and further treated with uranyl formate aqueous solution (15 μL, 1% (w/v)) for 20 s. Grids were imaged on a Tecnai Spirit microscope at 80 kV.

Dynamic light scattering

Liposomes:protein complexes (31:1 lipid:protein ratio) were incubated overnight at room temperature, diluted 60 times and their size was measured using a nano-ZS zetasizer instrument.

Circular Dichroism

Protein secondary structure was assessed by measuring the circular dichroism spectra on a Chirascan V100 (Applied Photophysics) equipped with a Peltier controller. Samples containing ApoL-III (5 μM) and Nplp2 (10 μM) alone or with DMPC liposomes (at a 31:1 molar ratio) were acquired at 24°C, unless otherwise stated.

Generation of Nplp2 deficient flies

Nplp2^{SK} stock was generated using the CRISPR/Cas9 technique as previously described (Kondo and Ueda, 2013). The following gRNA sequence was used GTCCGCCCGCGTCCCCCGTGAGG. Eight mutant candidates derived from male parents carrying nos-Cas9 and U6-gRNA transgenes were screened by PCR and direct sequencing of the target region. Nplp2^{154} and Nplp2^{156} mutants were generated as previously described by (Lee et al., 2014) Briefly, gRNA were synthesized *in vitro* using the GeneArt precision synthesis kit (ThermoFisher) and purified following the manufacturer's instructions. 300ng of *Nplp2* gRNA and 300ng of *ebony* gRNA were mixed with 4.5 μg of GeneArt Cas9 Platinum (ThermoFisher) in 10mM Tris pH7.8, incubated 15min at 37°C and microinjected into w^{1118} embryos. G_0 ebony$^-$ mosaics flies were selected and crossed to w^{1118};TM6c/Xa flies and F_1 were screened by T7 endonuclease assay (Lee et al., 2014). Homozygous mutant F_2 flies were validated by PCR and sequencing of the target region. gRNA sequences were: ebony: TCTTCGAGGAGCAGCAGCTGCGG; Nplp2^{154}: GTCCGCCCGCGTCCCCCGTGAGG; Nplp2^{156}: a 1:1 mixture of GCTCCGTAGCTCTAAACGCTCGG & GTCCGCCCGCGTCCCCCGTGAGG. PAM sites are underlined.

Generation of transgenic flies

Nplp2 sequence containing the 5′UTR and the coding sequence without stop codon was synthesized (Life Technologies) and cloned into a pDONR221 vector. This construct was then swapped into either pPWH destination vector to make *UAS-Nplp2-HA* or pTWG destination vector to create *UAS-Nplp2-GFP*. Transgenic flies were established by standard *P* element-mediated germline transformation. At least three independent lines of each construct were tested for expression level. Nplp2 genomic sequence was cloned into p[ACMAN]-attB vector and inserted by PhiC31-mediated recombineering at Bestgene inc.

Quantitative PCR

For quantification of mRNA, 10 wandering L3 larvae were collected and total RNA was isolated by TRIzol reagent and dissolved in RNase-free water. 500ng total RNA was then reverse-transcribed in 10 μL reaction volume using PrimeScript RT (TAKARA) and a mixture of oligo-dT and random hexamer primers. Quantitative PCR was performed on cDNA samples on a LightCycler 480 (Roche) in 96-well plates using the LightCycler 480 SYBR Green I master mix. Primers used were: Rp49_F: TCTGCATGAGCAGGACCTC; RP49_R: ATCGGTTACGGATCGAACAA; Lpp_F: CACCAGTAAAGGGGCTCTCA; Lpp_R: CCAGCCACCGTTATTAAGGA; LTP_F: GGCGCAGAGCTTCTTTAGTG; LTP_R: CGCTGATCGAAGGTCATGTA

Histology and immunostaining

Larval tissues were dissected in PBS, and fixed for at least 1 h at room temperature in 4% paraformaldehyde in PBS. Guts were stained with Bodipy^{TM} 493/503 (Life Technologies) for 30min, washed in PBS and mounted with DAPI. For immunostaining, after fixation, tissues were subsequently rinsed in PBS+0.1% Triton X-100 (PBT), permeabilized and blocked in 2% bovine serum albumin PBT for 1 h, and incubated with primary antibodies in 2% bovine serum albumin PBT overnight at 4 °C. After 1h washing, secondary antibodies and DAPI were applied at room temperature for 2 h. Primary antibodies used are as follows: mouse anti-Arm (DSHB, 1:100), chicken anti-GFP (Abcam, 1:1,000), anti-V5 tag (clone 25F11F7, ThermoFisher) ant anti-HA antibody (clone 3F10, Roche). Alexa488-, Alexa555- or Alexa647-conjugated secondary antibodies (Life Technologies) were used. Carcasses from 7-days old males were dissected and fixed in 4% paraformaldehyde overnight and subsequently stained with Bodipy^{TM} 493/503. Nuclei

were counterstained with DAPI (Sigma), and Alexa647 Phalloidin (Life Technologies) was used to stain F-actin in some experiments. All the images were taken on a Zeiss LSM 700 confocal microscope, except the whole guts that were imaged on a Leica M205FA binocular coupled to a DFC7000T camera. Images were processed using ImageJ.

Hemolymph proteins separation

Hemolymph samples were collected as follows: forty larvae were bled on a glass slide on ice, hemolymph was recovered and mixed with 10 μL of PBS supplemented with complete protease inhibitor solution (Roche) and 1mM phenylmethylsulfonyl fluoride (Sigma) and N-Phenylthiourea (Sigma) and centrifuged for 10 minutes at 1'000 g, 4°C, followed by a second centrifugation 5min at 10,000 g. Protein concentration was measured by BCA. 200ug protein in 100μL PBS were mixed with 900μl 0.5g/mL KBr solution and overlaid with 900μl 0.9% NaCl. Samples were centrifugated at 46200 rpm for 14h in a SW55Ti rotor. 100μl fractions were collected and precipitated by chloroform:methanol extraction and subjected to western blot. Tx-114 partitioning protocol was adapted from (Jessen and Wulff, 2015). Briefly, 200ug of hemolymphatic proteins in 20μl of 50 mM tris, pH7.4 150mM NaCl (Buffer A)+ protease inhibitors were mixed with 14μl TX-114 10% solution (Pierce) and incubated 30min on ice. 38μL of buffer A containing 6% sucrose, 0.06% Tx-114 (buffer B) were added below the Tx-114-containing phase and incubated 5min at 37°C. The mixture was centrifugated 5min at room temp, 5,000 g and the upper, soluble phase was kept on ice. 42μl buffer A was mixed to the lower phase on ice, followed by addition of 38μl buffer B below and incubation at 37°C for 5min. The mixture was spun 5min at room temp, 5,000 g and the lower, detergent-phase was kept on ice for subsequent Western Blot analysis.

Ex vivo Hemolymph assay

Larvae were raised on a food containing 10% D-glucose, 10% Methanol:Chloroform-extracted yeast and 1% agarose supplemented with 6.2 μg/mL cholesterol. 55ul hemolymph adjusted to 8mg/mL was added to 80ul Grace's medium containing 20 guts of larvae fed a regular diet. Samples were incubated 4.5 hr at room temperature under gentle rocking. Supernatants were subjected to density gradient as describe above, desalted using a 96-wells Zeba^{TM} spin plate (Thermo Scientific) and subjected to Western Blot.

Western blotting

Twenty guts or fat bodies from wandering L3 larvae were dissected and homogenized in RIPA buffer supplemented with protease inhibitors using a Precellys 24 homogenizer (Bertin Technologies). Homogenates were spun 10min at 1000 g and supernatants were centrifuged 30min at 13000 g, 4°C. Protein concentration of the samples was determined by BCA assay and 40 μg of protein extract was separated on a 4%–12% acrylamide precast Novex NuPage gel (Invitrogen) under reducing conditions and transferred to nitrocellulose membranes (Invitrogen iBlot). After blocking in 5% non-fat dry milk in PBS containing 0.1% Tween-20 for 1 h, membranes were incubated at 4°C overnight with a mouse anti-GFP antibody (Roche) in a 1:1500 dilution, mouse anti-Myc tag antibody at 1:1000 dilution (clone 9E10, Millipore), HRP-coupled-mouse-anti-HA tag (clone 6E2, cell signaling) or a rabbit anti-Lipophorin antibody (kind gift of Dr. Suzanne Eaton) in a 1:1000 dilution. Donkey anti-mouse-HRP, anti-rat-HRP or anti-rabbit-HRP secondary antibody (Jackson ImmunoResearch) in a 1:15'000 dilution was incubated for 45min at room temperature. Bound antibody was detected using ECL (GE Healthcare) according to the manufacturer's instructions. Membranes were imaged on a Fusion FX7 (Vilber Lourmat) and band intensity was quantified using ImageJ software.

Peptide fraction preparation

Peptide fraction extraction protocol was adapted from (Verleyen et al., 2006). Briefly, 0.5 mL of wandering L3 were crushed in 20μl of 50X complete protease inhibitor (Roche), centrifuged 2min at full speed. 130 μL of supernatant was mixed with 520 μL of methanol: H2O:formic acid (99:9:1 v:v:v) and vortexed 15sec. This mixture was sonicated in a water bath filled with water and ice for 15min and centrifuged at full speed for 12min. 500 μL of supernatant was dehydrated and resuspended in 300 μL H2O/0.1% trifluoroacetic acid and an equal volume of ethylacetate was added. After centrifugation, the lower was dehydrated and kept for MS analysis.

LC-MS/MS analysis

Peptide extracts were desalted on C18 StageTips according to Rappsilber et al. (Rappsilber et al., 2007) and evaporated to dryness in a vacuum concentrator. Desalted peptides were reconstituted in 20 μL Buffer A (2% acetonitrile (ACN)/98% H2O, 0.1% formic acid (FA)). LC-MS/MS analysis was performed at the Protein Analysis Facility (University of Lausanne). Around 1μg of total peptides was loaded on an Acclaim PepMap100 C18 (100 μm ID x 20 mm, 5 μm, Dionex) precolumn and separated an on analytical column (75μm ID x 15 cm, 3.0μm, 120 Å, Nikkyo Technos, Japan) on a Dionex Ultimate 3000 RSLCnano System (Thermo Fisher Scientific) coupled with an Orbitrap Fusion mass spectrometer with ETD fragmentation option (Thermo Fisher Scientific). Peptides were separated at a flow rate of 300 nL/min using a succession of linear gradient steps from 3 to 10% solvent B (80% ACN, 0.1% FA) in 10 min, followed by a 75 min step to reach 30% solvent B, a 13 min step to reach 50% solvent B, a 5 min step to reach 95% solvent B that was maintained for 5 min. Each sample was run for 140 min, including sample loading and column equilibration times. Data was acquired using an data dependent acquisition mode (DDA) with the decision tree option available in Xcalibur activated. Two methods were used to acquire the data. Method 1 combined ETD fragmentation for peptide ions with charge state 4 to 8 and HCD fragmentation for doubly and triply charged peptides when higher charge states were below a certain threshold. In Method 2 ETD was replaced by ETD with

supplemental activation (EThcD) to increase the dissociation of gas phase fragments while doubly and triply charged peptides were fragmented with HCD in the collision cell. For each method the cycle time was set at 3 s.

MS1 Spectra were measured with a resolution of 120,000, an AGC target of 3e6 and a mass range from 350 to 1550 m/z. Up to 10 MS2 spectra per duty cycle were triggered at a resolution of 15,000, an AGC target of 1e6 and an isolation window of 1.6 m/z in either ETD (resp EThcD) or HCD with a normalized collision energy of 30.

All the raw LC-MS/MS data were subjected to Peaks Studio 8.5 (BSI, Canada) for data refinement and spectral interpretation. Refined data were successively subjected to DeNovo, PeaksDB, PeaksPTM and Spider search using the *Drosophila melanogaster* reference proteome database with isoforms (AUP000000803_180220) with decoy database to control the FDR. The mass tolerance of precursor resp product ions was set at 7 ppm and 0.02 Da for PeaksDB search with amidation (C-terminal), acetylation (protein N-terminal), pyroglutamylation from Gln (N-terminal) and oxidation for methionine set as variable modifications. Candidate neuropeptides were systematically validated by manual inspection of spectra.

Lipids measurements

20 larval guts or fat bodies or carcasses from 20 males were dissected in 120 μΛ PBST, homogenized in a Precellys 24 homogenizer. Hemolymph was collected on ice by bleeding 20 larvae in PBS and debris and hemocytes were removed by centrifugating the hemolymph 5min at 13000rpm. All samples were inactivated at 70°C for 10min. Samples were then centrifuged at 13000rpm for 3min. 20 μL aliquots of the supernatant were assessed in 96-wells plates with the Triglyceride reagent and Free Glycerol Reagent (Sigma). 50 μL of supernatant were measured using Amplex Red Cholesterol determination kit (Sigma).

Lipidomics

Lipids from fat body FB, Hemolymph HL, and Gut *Drosophila* larvae, were extracted using a modified version of the Bligh and Dyer (Bligh and Dyer, 1959) protocol. Briefly, 500μL of methanol were added to the tissue and shaken for 2min. After addition of 400μL of chloroform and vortexing for 1min, the mixture was centrifuged at 4°C for 3min at 2000 x g and the lower phase was collected. 400μl of chloroform was added to the aqueous phase for a second extraction. The pooled organic phase was vacuum dried for 20min (ScanVac, Labogene) and solubilized in 100μL chloroform/methanol 1:2 (v/v) before analysis.

Lipid extracts were separated on a HILIC Kinetex column (2.6um, 2.1 × 50mm) on a Shimadzu Prominence UFPLC xr system. Mobile phase A was acetonitrile/methanol 10:1 (v/v) containing 10 mM ammonium formate and 0.5% formic acid. Mobile phase B was deionized water containing 10 mM ammonium formate and 0.5% formic acid. Gradient flow elution at 200μL/min began at 5% B with a linear increase to 50% B over 7 min; the 50% B were held for 1.5 min and lastly the column was re-equilibrated for 2.5 min. Sample solvent was chloroform/methanol 1:2(v/v), of which 2μL were injected.

Data were acquired in full scan mode at high resolution on a hybrid Orbitrap Elite (Thermo Fisher Scientific, Bremen, Germany). The system was operated at 240'000 resolution (m/z 400) with an AGC set at 1.0E6 and one microscan set at 10 ms maximum injection time. The heated electro spray source HESI II was operated in positive mode at a temperature of 90°C and a source voltage at 4.0KV. Sheath gas and auxiliary gas were set at 20 and 5 arbitrary units respectively while the transfer capillary temperature was set to 275°C. Mass spectrometry data were acquired with LTQ Tuneplus2.7SP2 and treated with Xcalibur 4.0QF2 (Thermo Fisher Scientific). Lipid identification was carried out with Lipid Data Analyzer II (LDA v. 2.5.2, IGB-TUG Graz University) (Hartler et al., 2011). The LDA algorithm identifies peaks by their respective retention time, m/z and intensity. Care was taken to calibrate the instrument regularly to ensure a mass accuracy consistently lower than 3 ppm thereby leaving only few theoretical possibilities for elemental assignment. Data visualization was improved with LCMSexplorer in a homemade web tool hosted at EPFL (https://gecftools.epfl.ch/lcmsexplorer/login)

QUANTIFICATION AND STATISTICAL ANALYSIS

Bioinformatics and structural prediction

Nplp2 multiple sequence alignment was performed and visualized using Geneious software. Nplp2 sequence without signal peptide was submitted to HHblit and the alignment of the ten first hits was used to detect protein homology using HHPred. A homology-based structural model was built using Modeler implemented in MPI bioinformatics toolkit webserver using the coordinates of the NMR structure of *Manduca sexta* Apolipophorin-III as a template (Wang et al., 2002) (PDB: 1EQ1). The structural figures were generated using PyMol (https://pymol.org/2/). Helical wheel projections were made using an online tool (http://rzlab.ucr.edu/scripts/wheel/wheel.cgi).

Statistical analyses

Each experiment was repeated independently a minimum of three times (unless otherwise indicated), error bars represent the standard error of the mean of replicate experiments. Data were analyzed using appropriate statistical tests as indicated in figure legends using the GraphPad Prism software. P values are represented in the figures by the following symbols: ns for $p \geq 0.05$, * for *P* between 0.01 and 0.05; ** for P between 0.001 and 0.01, *** for $p \leq 0.001$.